Laser Scanning Based Autostereoscopic 3D Display

by

Erdem Erden

A Thesis Submitted to the
Graduate School of Sciences and Engineering
in Partial Fulfillment of the Requirements for
the Degree of

Master of Science

in

Electrical and Computer Engineering

Koç University

June 2010

Koç University
Graduate School of Sciences and Engineering

This is to certify that I have examined this copy of a master's thesis by

Erdem Erden

and have found that it is complete and satisfactory in all respects,
and that any and all revisions required by the final
examining committee have been made.

Committee Members:

_____
Hakan Urey, Ph. D. (Advisor)

_____
Murat Tekalp, Ph. D.

_____
Alper Kiraz, Ph. D.

Date: 22.06.2010

ABSTRACT

This thesis presents a novel technical solution to the laser projection part of an autostereoscopic (i.e. no glasses) 3D display system that is developed within a consortium of eight partners. The system includes a high accuracy and low latency pupil-tracking module which enables formation of dynamic exit pupils. The image is sent to the viewer by direct projection of red, green and blue lasers via a low loss transparent screen. The use of lasers provides the display a high color gamut.

The display optics compromises two basic functional units: the Light Engine and the Transfer Screen. The image is formed by scanning a line shaped laser beam over a liquid crystal on silicon (LCOS) device at the Light Engine part of the display. The location of the exit pupil is adjusted at the transfer screen part of the display with the help of a spatial light modulator (SLM) and stereo images are directed to the corresponding eyes after passing through a special transparent screen.

The major contributions of this thesis are optical design and analysis of the display system via the commercial optical design tool, ZEMAX, beam combining, beam shaping and beam homogenization of lasers with single and multiple emitters and development and fabrication of a laser scanning projection unit as part of a novel 3D display system.

ÖZET

Bu tez, sekiz adet partnerin ortaklığıyla geliştirilmiş, herhangi bir özel gözlük gerektirmeden üç boyutlu görüntü sağlayan lazer temelli bir televizyon sistemi için yeni bir lazer temelli izdüşüm sistemi sunmaktadır. Geliştirilen sistemde, göz bebeği takip sistemi sayesinde çıkış açıklığı faal olarak ayarlanarak üç boyutlu görüntü kullanıcıya sağlanmaktadır. Düzenek, geri beslemeli şekilde çıkış açıklığını ayarlamasını sağlayan yüksek duyarlığa ve düşük cevap verme süresine sahip yüz tanıma birimi içermektedir. Tasarlanan görüntüleme düzeneğinde sol ve sağ göze gönderilecek çiftli görüntüler birbiri ardına çoklu kullanıcı için oluşturulmakta ve uygun gözlere gereken şekilde iletilmektedir. Oluşturulan görüntü izleyiciye kırmızı, yeşil ve mavi lazerlerin verimliliği yüksek geçirgen bir ekran üzerinden doğrudan yansıtılmasıyla gönderilmektedir. Lazerlerin kullanılması görüntüleme sistemine geniş bir renk gamı kazandırmakta ve oluşturulan canlı ve gerçekçi görüntüler sayesinde zengin bir kullanıcı deneyiminin oluşması sağlamaktadır.

Görüntüleme sisteminin optik kısmı, Işık Motoru ve İletim Ekranı olmak üzere iki temel işlevsel bölüme ayrılmaktadır. Düzeneğinin Işık Motoru bölümünde bir lazer ışını çizgisinin silikon üzeri sıvı kristal yapılı (LCOS) bir aygıt üzerinde taranmasıyla görüntü oluşturulmaktadır. Düzeneğin çıkış açıklığının konumu, uzamsal bir ışık ayarlayıcı (SLM) sayesinde iletim ekranı bölümünde ayarlanmaktadır. Sol ve sağ göz için oluşturulan görüntüler ilgili gözlere özel geçirgen bir ekrandan geçtikten sonra iletilmektedir.

Bu çalışmanın temel katkısı, görüntüleme düzeneğinin tasarımının ve tahlinin optik tasarım yazılımı ZEMAX ile yapılması, lazer ve lazer dizinleri için ışın birleştirme, şekillendirme ve bir örnek aydınlanma sağlanması işlemlerinin yapılması ve yeni bir üç boyutlu televizyon için lazer izdüşüm bazlı bir görüntü oluşturma düzeneğinin tasarlanması ve üretilmesi aşamalarında olmuştur.

ACKNOWLEDGEMENT

Foremost, I would like to thank my thesis advisor Prof. Hakan Urey for providing his continous support, invaluable guidance and brilliant ideas throughout my study at Koç University. His knowledge, continuous encouragement and trust on me have taken the major role in the development of my research skills. I would also like to thank Prof. Murat Tekalp and Prof. Alper Kiraz for kindly taking part in my thesis committee and providing their invaluable insight.

I would like to express my gratitude to 7th Framework Programme of EC for funding the project and all Helium3D partners especially Dr. Eero Willman, Hadi Baghsiahi, Prof. Sally Day, Prof. David Selviah and Prof. Anibal Fernandez from UCL and Prof. Phil Surman from DMU for their support and valuable feedback.

I acknowledge TUBITAK for granting the graduate student fellowship for my master's degree studies.

I would like to thank all the past and present members of OML for their support and help. I am honored to be one of the members of this laboratory and had a chance to work with you. I would like to sincerely thank my project partner Dr. Kishore V.C. for providing his valuable insight and Selim Ölçer for his continous support and providing his bright ideas whenever I got stuck.

My dear collegues and friends S. Kutal Gökçe, Onur Ferhanoğlu, Duygu Kutluoğlu, Hüseyin R. Seren, Aslıhan Arslan, Gökhan Hatipoğlu, Burak Erarslan, Pelin Ayerden and Ersin Hüseyinoğlu: It was a privilege to work with you and without your continuous help, support and jokes (especially Kutal, Ersin and Onur) this work would not be possible.

My long time friends İbrahim Kamer and Emre Sancak. Even though we were not always together, you were always there whenever I needed your help. Thanks for everything.

Last, but definitely not the least, I would like to thank to my parents, my sister Evrim, her husband Serkan and my lovely niece Eylül for their never ending support and caring. To them, I dedicate this thesis.

LIST OF FIGURES

LIST OF TABLES

Table of Contents

1 INTRODUCTION

The developments in lasers and display technologies have led to major changes in the display devices and a large number of new commercial products and advanced prototypes have been launched at various trade shows. The display industry is witnessing a major change over from mere 2D to more realistic 3D with improved efficiency and color quality. It can be envisioned that within the next few years a major share of the current displays will be replaced by 3D capable displays.

The human brain extracts the depth information and perceives the stereoscopic views by fusing together the two images acquired by the eyes. The binocular disparity is the disparity in these two images and it is a widely utilized visual cue to render a stereoscopic view in displays. Although this requirement had been understood by Euclid around 300 BC, the first stereoscopic device appeared in 1832 when Charles Wheatstone introduced the stereoscope [1]. A stereoscopic image can be produced by using many different technologies ranging from simple anaglyph methods to advanced autostereoscopic and interactive techniques.

Even though the idea of using lasers for displays was proposed in the 1960's [2], the availability of compact, efficient and low cost lasers emitting red, green and blue colors, triggered the recent development of laser based displays. An immediate advantage of using spectrally pure laser light for displays is the wide color gamut it can produce. Lasers combined with different type of modulators, scanners and optical components can be used to build various display systems including 3D displays.

The state of the art in 3D displays providing examples of commercially available products wherever possible is given in the sections below. A discussion of the performance

of different displays and the contribution of this thesis to the current technology are given in the end of the section.

The classification of current 3D display technologies is shown in Figure 1.1[3].

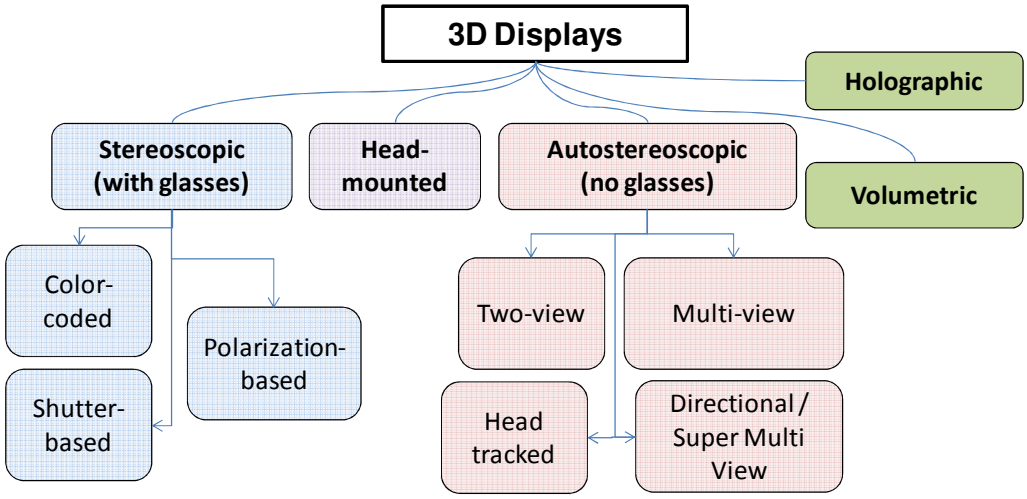

Figure 1.1 The classification of current 3D display technologies

1.1 Stereoscopic Displays

The 3D displays which require the viewer to wear special glasses in order to perceive 3D can be divided into three main categories.

1.1.1 Color Coded Displays

Using anaglyph glasses is a classic method of creating color multiplexed 3D visualization. This is an inexpensive solution to the 3D visualization problem and can be applied whenever common color video equipment is available. Anaglyph 3D images are produced by combining the images for the left and right eye using a complimentary color coding technique. The most common is the anaglyph with the red channel for the left eye

and the cyan channel for the right eye. The viewer wears a pair of colored glasses so that the left and right eyes receive the corresponding images only. Main drawbacks of this type of display are the loss of color information and the high degree of crosstalk. Spectral responses of the display and the anaglyph glasses, the transmission protocols and the image encoding have been cited as the sources of crosstalk [4]. The crosstalk between the left and the right eye images causes a ghosting effect that decreases the perceived image quality.

In order to increase the quality of the images by reducing the crosstalk, the red component from the left image can be aligned with the green and the blue components from the right image [5]. Other methods such as stereo pair registration, color component blurring and depth map adjustments have also been demonstrated with substantially reduced image quality issues [6]. A sample of anaglyph image with and without enhancement can be seen in Figure 1.2. Although it is the least expensive and one of the oldest 3D viewing techniques, anaglyph is not widely preferred when high image quality is a priority.

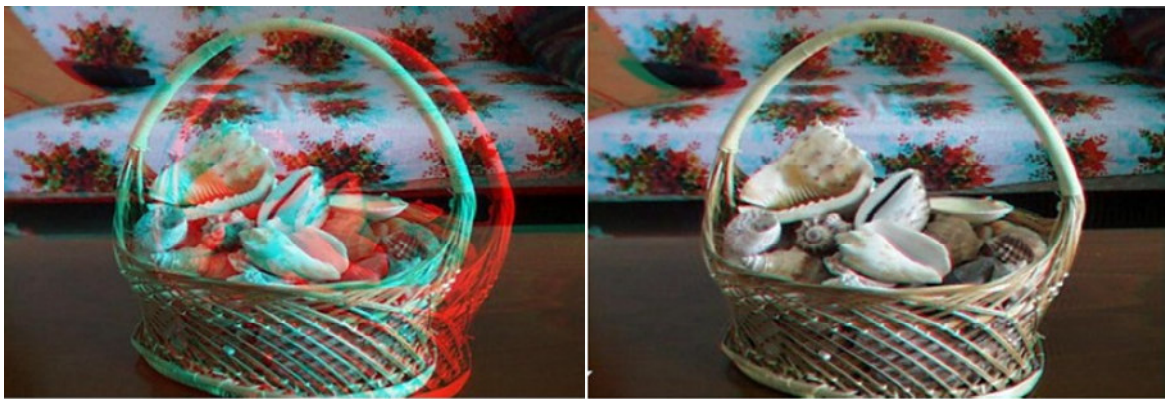

Figure 1.2 Photo of the standart color anaglyph (left) and the anaglyph enhanced with image registration (right) [6]

1.1.2 Polarization Based Displays

In polarization based displays, the state of polarization (SOP) of the light corresponding to each image in the stereo pair is made mutually orthogonal. Linear or circular polarization can be employed, but the latter has the advantage of the absence of crosstalk if the viewer's head is tilted. The viewer uses eyewear with appropriate polarizers to direct to images to the corresponding eyes. Images are produced by a two-projector setup in which projectors produce images that has orthogonal polarization states. This type of displays requires the use of a special screen that preserves the state of the polarization. For rear projection, a combination of Fresnel-lenticular surface can be used for preserving the SOP while for front projection, a silver screen is used.

The use of two projectors increases the complexity and cost of the display system and causes problems in alignment. A single projector equipped with an electrically controllable polarization rotator synchronized to the frames being displayed can be used to solve this problem [7]. This method is cost-effective and requires no alignment but since the rotators have a finite response time, blanking is necessary between the left and right images for reducing crosstalk and that leads to light loss. Another alternative to double projector configuration is employing a single projection unit that can produce two full color images with orthogonal polarization states by a single modulation unit [8, 9]. The described single projection unit has a LED illumination unit shown in Figure 1.3. The two full color images with orthogonal polarization states are generated by a single modulation unit containing four LCOS devices (two for each eye) and some polarization controlling optics.

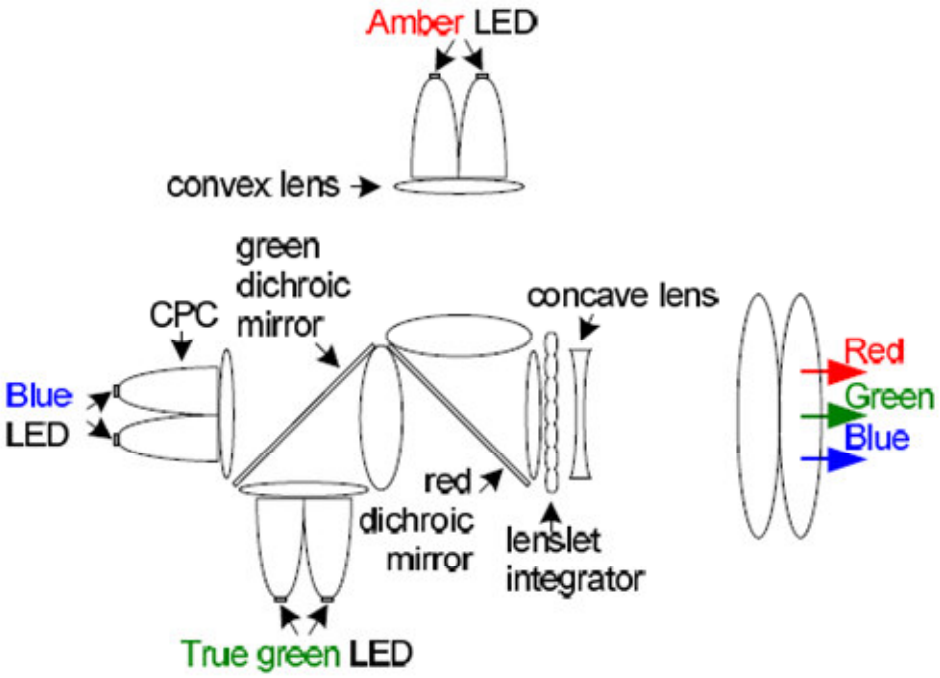

Figure 1.3 Illustration of the polarization based single projection display's illumination system. The display uses multiple LED sources with red, green and blue colors[8]

Polarization multiplexed 3D displays offer higher image resolution and color quality compared to anaglyph-based displays. On the other hand, ghost images, hot spots or abrupt fall-off of intensity that can be caused by the deteriorations in the projection lens or the screen and the chromatic aberrations caused by the polarizing filters decreases the image quality of polarization multiplexed 3D displays.

1.1.3 Shutter Based Displays

The shutter based displays exploit the persistence of vision of the human visual system to give 3D perception. In this technique, the left and the right eye images are displayed on the screen in an alternating fashion at high frame rates (usually 120 Hz). This is referred as the alternate frame sequencing and the viewer is required to wear battery powered active

shutter glasses which are synchronized to the content being displayed. The synchronization can be done by using an infrared emitter, radio frequency, Bluetooth or by the so-called DLP Link (Texas Instruments) which uses encoded white light flashes detected by the shutter glasses in between the left and the right frames. The liquid crystal-based glasses block the left eye images from reaching the right eye of the viewer and vice versa. The disadvantages of this type displays are the cost of the active shutter glasses and the high video bandwidth requirement.

1.2 Head Mounted and Interactive Displays

At present, systems with the capability of interaction with the displayed images are part of expensive training or research facilities. As the technology advances, such systems might become more affordable and a trend similar to the current 3D boom might set off in the future. This section briefly discusses the techniques and progresses in head mounted and interactive displays.

1.2.1 Head Mounted Displays

Head mounted stereoscopic displays (HMDs) are binocular systems with two separate image generators and employ relay optics [10]. These displays are head worn by the user so the mobility is available without interrupting the 3D view and a feeling of immersion in the scenes being displayed can be given. This technology is widely used for training purposes in the medical, military and industrial fields by producing a virtual environment.

In HMDs, the video see-through approach is considered to be better than the optical see-through approach since superimposing the real world images acquired through a video camera with the virtual world information from a computer has less complexity compared with the precision eye-pupil tracking required for optical see-through [11]. The video see-through approach is successfully implemented in the medical field [12] and a Computer

Aided Surgery (CAS) system in which the surgeons can have detailed computer-generated information superimposed on patients in real time is shown in Figure 1.4.

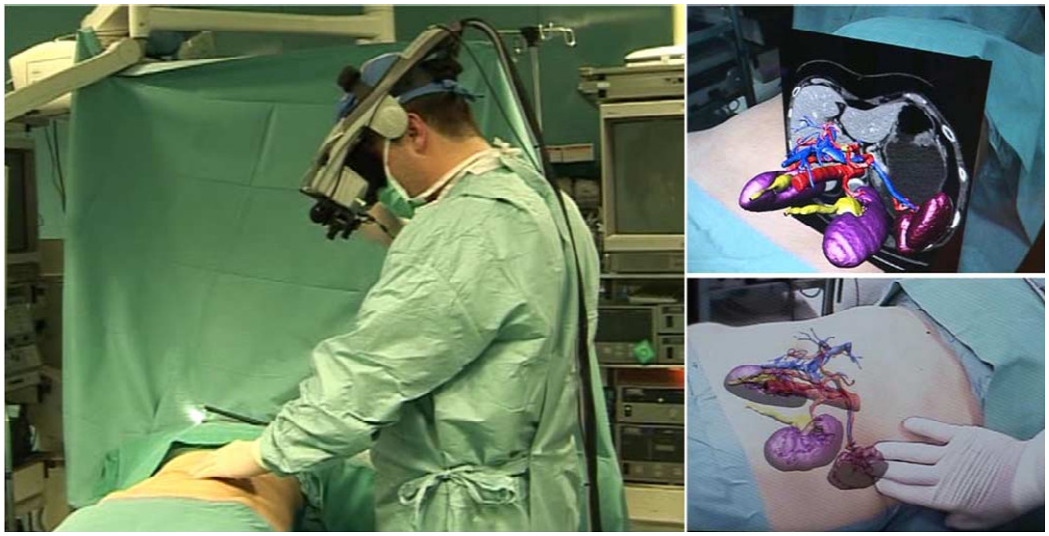

Figure 1.4 A Computer Aided Surgery (CAS) system (left) and the mixed reality views through the HMD (images on the right) [12]

Achieving large field of view (FOV) and resolution simultaneously is one of the major problems in HMDs. Optical tiling, presenting a high resolution small inset image and a low resolution background based on user pupil tracking are some of the solutions proposed to address the requirement of high FOV and high resolution [13-15].

Similar to many 3D display technologies, 3D-HMDs also have the problem of accommodation-convergence (AC) mismatch. AC mismatch occurs when the eyes focus at the screen but converge at the apparent distance of the point of fixation. In order to eliminate AC mismatch, task-specific multiple image locations can be created. Systems that can form images at different planes by using moving parts [16] or no moving parts [14] have been proposed.

One of the main challenges associated with the development of 3D-HMDs display is the visual discomfort due to the possible differences in the left and right eye images. HMDs utilize two separate displays; thus mismatch in any of the optical properties or alignment of the components used in the optical train of the left and right channels become critical [17, 18]. Other challenges and problems related to the optical design of HMDs can be found in the literature [19].

1.2.2 Interactive 3D Displays

After providing the user with a realistic stereoscopic view, the next step is giving the user the opportunity of interacting or touching those virtual objects. Haptic interaction with the displayed objects is enabled by the use of devices that have an interaction point. When the user interacts with the haptic device, it generates the force feedback with the help of algorithms [20]. One of the early interesting interactive displays is a WYSIWYF (What You See Is What You Feel) display [21]. Although not stereo capable, the viewer can interact with a computer generated model by using this technology. The display employs video see-through so that the viewer can reach for the object behind the display with his/her hand and feel the force of interaction while seeing his/her hand interact with the object on the display.

Stereoscopic versions of the idea above have also been implemented. Systems such as nanoWork bench [22] and the ALIVE system [23] are examples of stereoscopic interactive displays. Integration of 3D displays with other interfaces is seen as a key new research direction that will bring together researchers from different disciplines. For example, combining haptic techniques with holography is an interesting area where a lot of research activity is taking place [24, 25].

1.3 Autostereoscopic Displays

Autostereoscopic displays create stereoscopic images at exit pupils without requiring any form of special glasses or other user-mounted devices. Two-view (binocular) and multi-view systems with fixed viewing zones, head/pupil tracked and directional displays and super multi view (SMV) systems are different types of autostereoscopic displays which will be discussed in detail in the following sections. In two-view displays only a single stereo pair is displayed whereas in multiview displays multiple stereo pairs are produced to provide 3D images to multiple users. In autostereoscopic displays screen sized Fresnel lenses, lenticular arrays, parallax barriers or other components like holographic elements, mirrors, micro-polarizers and prisms are used to control light path and to form exit pupils. In autostereoscopic displays with fixed viewing zones, these components are used to create fixed exit pupils for viewer's left and right eyes. On the other hand, head/pupil tracked displays create exit pupils according to the viewer's eye pupil locations and enable the viewer(s) to see stereo comfortably without having to remain stationary. In directional and super multi-view systems, a large number of views are produced in order to create a smooth motion parallax across the viewing field.

1.3.1 Two-View Autostereoscopic Displays

Two-view systems are 3D-displays where a single pair of parallax views is produced. In two-view systems, the stereo pair can be formed at a single location or the pair can repeat itself in multiple zones in space (i.e. multi-viewer). The viewer's eyes have to be in the correct location within the ideal distance to perceive a stereoscopic image. Two-view systems with a head tracker can provide the same stereo pair to a single viewer or multiple viewers and enable a greater freedom of movement.

1.3.1.1 Parallax Barrier Systems

LCD elements are commonly used in 3D displays since they offer good pixel position tolerances and high position stability, have carefully controlled glass thickness and can be successfully combined with different optical elements [26]. Image quality issues of 3D displays based on LCD panels and solutions to improve their performance are studied and can be found in the literature [27].

LCD elements and other pixilated emissive displays can be combined with parallax barriers in order to create a two-view auto-stereoscopic display. As it can be seen in Figure 1.5, left and right eye image columns are placed one after another on the display and the parallax barrier which is composed of black slits, allows light to pass only to the desired viewing zone. The system creates repeated viewing zones along the display; therefore it can also be used to create a multi-view system. Parallax barriers can be combined with polarizers to create reflective type displays by using silver screens [28].

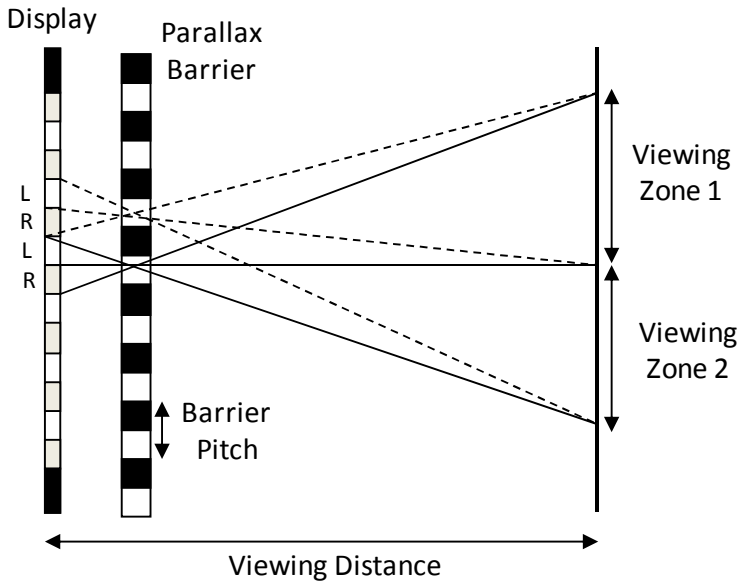

Figure 1.5 The illustration of a parallax barrier system. The parallax barrier which is composed of black slits, allows light to pass only to the desired viewing zone

In parallax barrier systems half of the pixels are used for each viewing zone and that leads to loss of brightness and spatial resolution. It is shown that the light efficiency and crosstalk level of a liquid crystal panel based system can be improved by using a slanted barrier [29]. Also using aperture grills instead of black stripes on an acrylic board as parallax barriers; increases the light efficiency by eliminating the reflection on the surface and provides better transmittance and contrast [30, 31].

Decreasing the display pitch in order to solve the resolution problem of the parallax barrier systems is not a useful option. The optimum viewing distance is proportional to the distance between the display and the parallax barrier and inversely proportional to the display pixel size. Therefore, as the display resolution gets higher, the optimum viewing distance of the system gets longer. In order to improve the resolution, the methods of using more than 2-views [32] and using two LCD elements have been proposed [33].

Parallax barrier systems can be 2D/3D switchable by removing optical function of the parallax elements [26]. The barriers can be optically switched by using polarization based electronic switching systems [34]. The improvements in OLED technology increased the usability of switchable 3D displays and Samsung announced a new 14" WXGA full resolution 2D/3D OLED display prototype with a fast switching parallax barrier [35].

Another use of parallax barriers is to combine them with projectors to create auto-stereoscopic 3D projectors [36] as it can be seen in Figure 1.6. The system is composed of multiple 2D projectors, a projection screen, and two parallax barriers. First parallax barrier controls the output of the projectors such that the size of image pixels on the projection screen is matched with the second parallax barrier's period. Second parallax barrier works as a regular parallax barrier and directs the parallax images to the viewers' eyes.

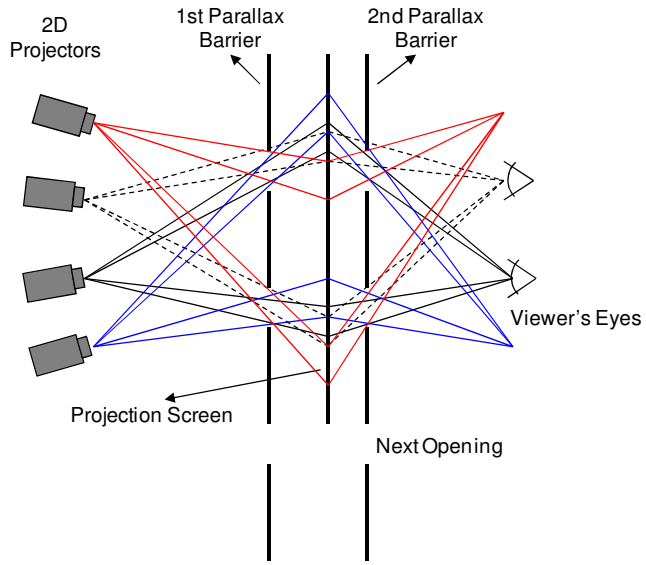

Figure 1.6 Illustration of a parallax barrier based autostereoscopic 3D projector. The system is composed of multiple 2D projectors, a projection screen and two parallax barriers. The first parallax barrier controls the output of the projectors and the second parallax barrier directs the parallax images to the viewers' eyes [36]

1.3.1.2 Lenticular Systems

Lenticular systems combine cylindrical lenses with flat panel displays to direct the diffused light from a pixel such that it can only be seen in a certain viewing angle in front of the display. The illustration of a lenticular system and the created viewing zones can be seen in Figure 1.7. Efficient lenticular lens design techniques, different analysis methods and recent advances in the technology can be found in the literature [37, 38].

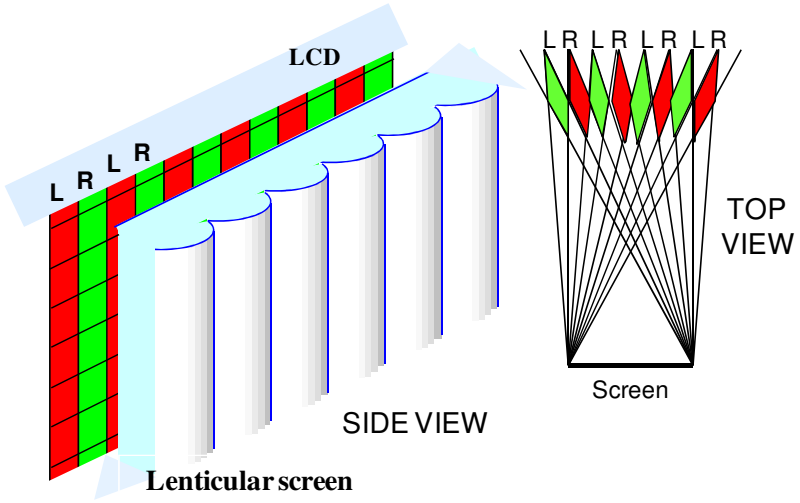

Figure 1.7 Illustration of the working principle of a lenticular screen. The same stereo pair repeats itself along the viewing zone.

The alignment of lenticular array on the display panel is a critical parameter in lenticular systems. The alignment gets more difficult as the display resolution increases and any misalignment can cause undesirable distortions in the 3D images. Software based solutions which will compensate production errors can be used to improve the quality of the lenticular systems [39]. Another problem with the lenticular systems is the intensity variation along the viewing zone due to beams coming from the sub-pixel regions of the display panels. As the viewer changes the viewing angle, pattern of dark and bright bands

are observed. This effect can be decreased by slanting the lenses and adjusting the focal length and the pitch of the lenticular array elements [40].

Similar to parallax barrier systems a lenticular display can be made 2D/3D switchable by using lenticular lenses filled with a special material (i.e. liquid crystal) that can switch between two refracting states [40]. The disadvantage of switchable lenticular displays compared to parallax barrier switchable displays is the residual lens affects at oblique angles even when the display is working in 2D mode.

1.3.2 Multi-view Autostereoscopic Displays

In multi-view displays with fixed viewing zones, multiple different stereo pairs are presented across the viewing field. User's left and right eyes lay in two adjacent regions which have different perspectives. The number of views in multi-view displays is too small for continuous motion parallax but different methods have been tried to keep the apparent image content close to the plane of the screen and minimize the sharp transitions between the views [41].

In the previous sections, it has been explained that parallax barriers and lenticular sheets can be combined with pixilated emissive displays to create repeated viewing zones along the display. In multi-view parallax barrier systems, more than two images can be created in the viewing zone by combining multiple videos together into a single video that can fit into the special step barrier [42, 43] or by using time multiplexing [44]. The problem that needs to be solved with lenticular systems in order to build multi-view lenticular systems is the reduction in resolution with the increase in the number of views. In vertically aligned lenticular arrays the resolution decreases in the horizontal direction only so the lenses should be slanted to distribute the resolution loss in two axes [40].

1.3.3 Head Tracked Displays

Head tracked displays (HTDs) can be divided into four main categories: Fresnel lens, lenticular, projection and parallax barrier systems. In addition, other techniques including prisms and holograms can be employed.

1) The earliest head tracking display with Fresnel lens was made by Alfred Schwartz where a pair of CRT projection modules projects the left and right images on to a Fresnel lens [45]. After this development, similar systems that use LCD displays have been built [33, 46].
2) Most of the lenticular HTDs use LCD panels to create images [47, 48]. Different masks can be applied to provide contiguous light across viewing field [49].
3) All projection stereoscopic displays operate on the principle of forming real images of the projector lenses in the viewing field. The projection displays can be divided into four categories according to their screen type and the categories can be listed as retro-reflecting [50], double lenticular screen [51], mirror [52] and lens systems.
4) In parallax HTDs, fixed physical barriers [53, 54] or dynamic parallax barriers [55] located in front of the display can be used to block the light from a pair of projectors that form exit pupils.

1.3.4 Super Multi-View and Directional Displays

A super multi-view (SMV) display is a multi-view display where the number of discrete images presented is sufficiently large to give the appearance of continuous motion parallax and to eliminate accommodation-convergence (AC) mismatch. The number of views required for this condition has been studied and reported [56-58].

In directional displays, discrete beams of light that vary with angle radiate from each point on the screen. Optical modules provide multiple beams that either converge or

intersect in front of the screen to form real image voxels or diverge to produce virtual voxels behind the screen. The screen diffuses the beams in the vertical direction only allowing vertical freedom of movement without altering horizontal beam directions. As the projectors/optical modules are set back from the screen, mirrors are situated either side in order to provide virtual array elements on either side of the actual array.

Directional displays maps the angles consistent with depth to voxels. Each screen pixel has a number of discrete emission angles controlled by the image generators behind the screen. Koç University, Istanbul, developed this concept by using an array of scanners made of standard printed circuit board (PCB) material [59]. Each scanner module carries an array of light emitting diodes (LEDs) on the moving platform as it can be seen in Figure 1.8 [60].

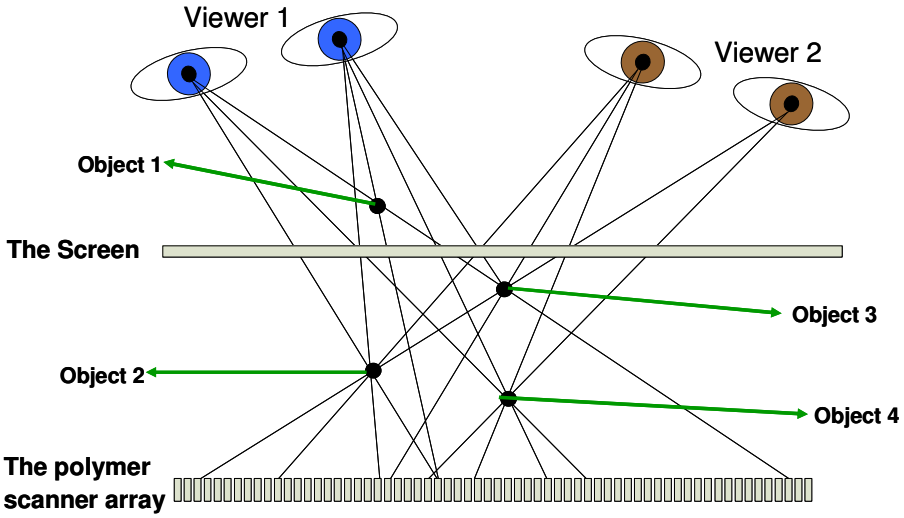

Figure 1.8 Directional display using a large array of FR4 scanners integrated with LED array and lenses [60]

1.4 Holographic and Volumetric Displays

Holography is the technique of capturing and reproducing the original wavefronts. This is the technology that can offer the most realistic autostereoscopic 3D since the images are formed in a physical volume by reproducing the original wavefronts and there are no problems of AC mismatch and loss of resolution and color quality. The limiting factors in this technology are the high resolution requirement on the display unit and the difficulty of creation, transmission and display of huge amount of data that is required.

Similar to the case of holographic displays, a positive aspect of volumetric displays is the absence of AC mismatch. Volumetric 3D displays mainly use either the swept volume method or the static volume method. In swept volume method, a projection surface rotates in 3D space reflecting light according to the synchronization signals and position thereby creating volume pixels (voxels). In the static volume method light is emitted from different points in the bulk of the volume when addressed. Advantages of volumetric displays are the very high FOV and the multi-viewer capability. One drawback is that the images are translucent.

There are many technological requirements for holographic or volumetric displays to be used widely as a consumer product; therefore these displays will not be discussed further here. A detailed discussion on the properties and drawbacks of these technologies can be found in the Special Issue of the Proceedings of the IEEE on "3D Media and Displays" which is expected to be published in 2011.

1.5 Contributions of the Thesis

3D displays have many applications and there are a large range of 3D demonstrators and products recently introduced to the market. The differences of the proposed 3D display

system from the described displays and its contributions to the state of the art in 3D displays are summarized below.

Helium3D is a 3D display which can support more than one viewer. The number of viewers is dependent on the speed of the light engine and the limitations are not optics related. It can provide 2D compatibility when it is desired or the number of viewers is more than the limit without any loss of image quality.

The user is not required to wear any special glasses so the loss of color in anaglyph displays or loss of brightness caused by the glasses are not problems of the Helium3D display. Also the display does not include any parallax barriers or polarizers to direct the images and the problems that have been explained related to these components have been eliminated.

The display incorporates a high accuracy, low latency pupil tracker so the viewer can see a 3D image without any restriction on the movement. The use of pupil tracking also adds the "look around" capability to the display. Helium3D will also address the interaction techniques in the near-field (distances within arm's reach of the display) which will increase its usability in the fields of medicine, gaming, engineering design etc.

One of the most important contributions of this display is the use of lasers as the light source. The lasers provide a very high color gamut display and the produced images have more lively and realistic colors.

Within the work of this thesis:

- Different types of lasers that can be used in displays have been analyzed.
- Power ratio calculation and white balancing of the display system have been completed.
- Different beam combining methods have been analyzed and designed.

- A new homogenization method including micro-lens arrays have been designed and implemented.
- The components required for beam shaping and combining have been designed and acquired.
- Opto-mechanic components for mounting the selected components have been designed and fabricated (when it is required) and acquired.
- The ZEMAX™ designs of the all Light Engine for the first and the second prototype have been finished.
- The complete optical hardware for Prototype 1 has been demonstrated.
- The required components for Prototype 2 have been chosen and acquired.

2 DISPLAY SYSTEM DESCRIPTION

The HELIUM3D (High Efficiency Laser-Based Multi-user Multi-modal 3D Display) is a joint research project with 8 partners and is funded by the EC 7th Framework Program. The project aims to extend the state of the art in autostereoscopic displays by developing a laser based, multi-view and multi-user display. The role of the Koç University in this project is to design and build the "Light Engine" part of the display. Other partners and their complementary roles are:

- De Montfort University: System integration and project coordination.
- Philips Electronics: Commercial applications, interaction and human factors.
- University College London: Optical design and simulation of the "Transfer Screen".
- BARCO: Stereoscopic systems and commercial applications.
- Heinrich Hertz Institute: Far-and near-field viewer tracking and interaction.
- Technical University Eindhoven: Human factors and interaction.
- Nanjing University: Near-field viewer tracking and interaction.

In this section, the description of the system architecture including the display hardware and the component selection will be given. The display is divided into functional blocks that have distinct inputs and outputs. During the project some of the components and some parts of the architecture were changed based on the experience gained and the available technologies. This section will summarize the specifications that were chosen at the first half period of the project.

2.1 Working Principle

As it is shown in Figure 2.1, the HELIUM3D display system consists of three sub-sections: the Light Engine, the Head Tracker and the Transfer Screen.

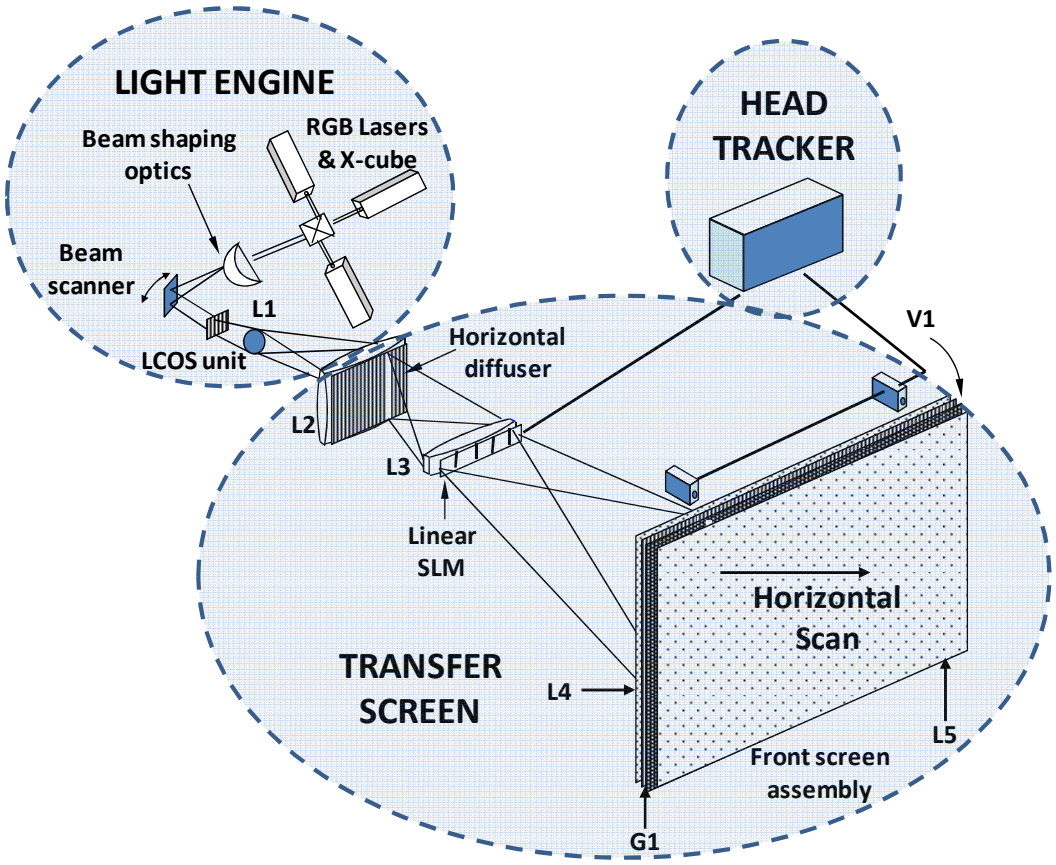

Figure 2.1 Schematic of the simplified Helium3D display hardware

The Light Engine [61, 62] combines red (R), green (G) and blue (B) lasers to produce a white light source with a low entendue. The light is shaped into a narrow vertical column using beam shaping optics. This laser line is scanned across a Liquid Crystal on Silicon

(LCOS) 2D light valve containing the image content in order to create a horizontally scanned columnar representation of the image. The figure is a simplified version of the actual display and only shows one light valve whereas the actual display employs three light valves with associated optics. The components producing the image are referred to as the Light Engine and can be considered as an entity whose purpose is to produce an image and project it onto lens L2 with the help of a conventional multi-element projection lens L1. The projection lens acts as an interface between the Light Engine and the Transfer Screen sub-systems of the display.

The locations of the viewers' left and right eyes are identified by the Head Tracker section of the display in real time [63]. The eye positions are used for controlling a ferroelectric liquid crystal spatial light modulator (SLM) within the transfer screen. The SLM steers the scanned image columns to the viewers' left of right eyes. The different modes of operation of the display (i.e. motion parallax, user-determined viewpoint, secure images visible only to selected viewer/s etc.) are realized with the help of this section of the display.

The remaining part of the display hardware is referred to as the Transfer Screen [64] and its purpose is to magnify the image on L2 and to control the direction of the light emerging from the front screen. L2 acts as a field lens and directs the scanned image column towards the center of the L3. The horizontal diffuser spreads the beam to cover the whole width of it. L3 projects the image formed on the intermediate image stage onto the surface of the front screen. The SLM is made of a large number of narrow vertical pixels arranged side-by-side along the horizontal axis. The states of the pixels can be controlled individually to form sections along the length of the SLM where it is either in transmission or extinction. These sections act as dynamically reconfigurable apertures whose sizes and

positions are continuously updated depending on the viewer positions and the angle of the scanning mirror during each image frame.

The position of an open aperture changes the angle at which an image is incident on the front screen. This angle determines the location of the exit pupil and as it can be seen in Figure 2.2, the images are sent to the desired eyes of the viewers. Left and right images are sent to the corresponding eyes by temporal multiplexing so a faster SLM is needed as the number of viewers is increased.

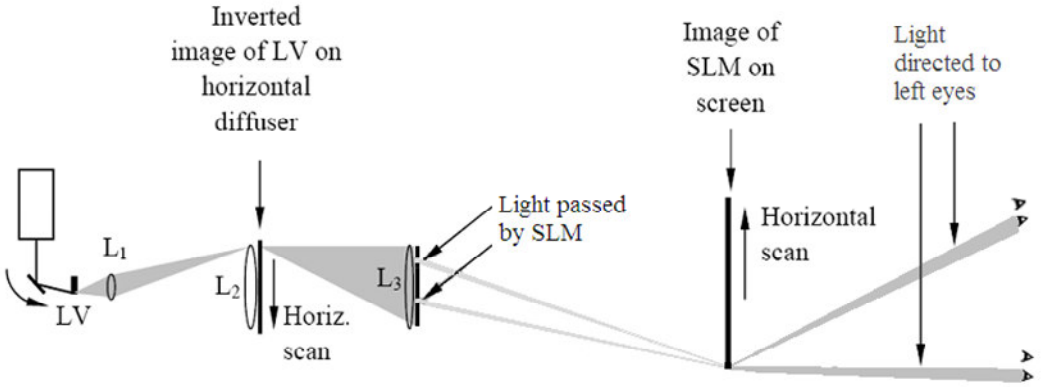

Figure 2.2 Top view of the display illustrating the dynamic exit pupil formation by the use of a SLM

The need for a scanning system is illustrated in Figure 2.3. In case 1, the viewer's eyes and the SLM are in the conjugate planes; therefore the dynamic SLM is unnecessary and the fixed openings are enough. In case 2, the user moves closer (or far away) from the screen during one frame time and the user's eyes are no longer at the image plane of the SLM. In order to send light to the viewer's eyes, the SLM opening needs to move dynamically during the frame time. In an area illumination system, the change in the location of the SLM openings changes the exit pupil location only in the image plane. The

scanning system allows the display to direct images to the corresponding eyes even the user moves closer or far away from the system.

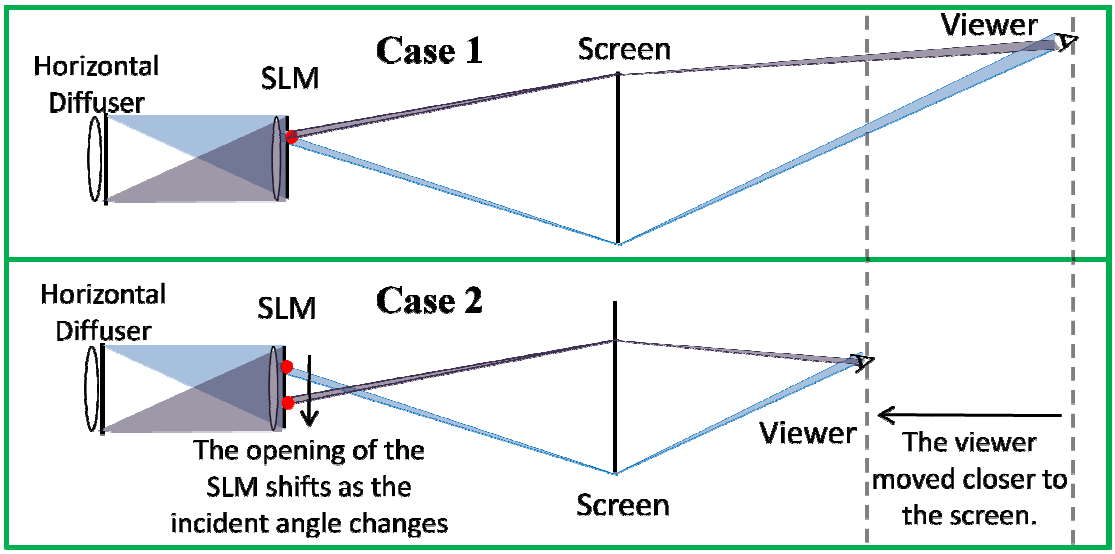

Figure 2.3 The exit pupil formation when the SLM and the viewer are at the conjugate planes (upper figure), and when the viewer changes location (lower figure). Two extreme scan angles are shown with different colors

The front screen consists of four different layers. Lenses L4 and L5 are aspherical Fresnel lenses, G1 is a cylindrical Gabor Superlens and V1 is a vertical diffuser. L4 collimates the transmitted light so that the axes of the diverging beams enter the superlens assembly orthogonally to its surface. After this, the superlens screen acts as a beam deflector with gain, magnifying the angular deviation caused by the SLM aperture by a factor of M. Lens L5 is a field lens that focuses the transmitted beams back toward the optic axis of the system. The focal length of lens L5 affects the range of viewing distances from the front screen where the whole image is visible. A shorter focal length allows the viewers to be located closer to the display and vice versa. Finally, the vertical diffuser V1 increases the size of the exit pupil in the vertical direction.

2.2 System Architecture

The block diagram of the system architecture is shown in Figure 2.4

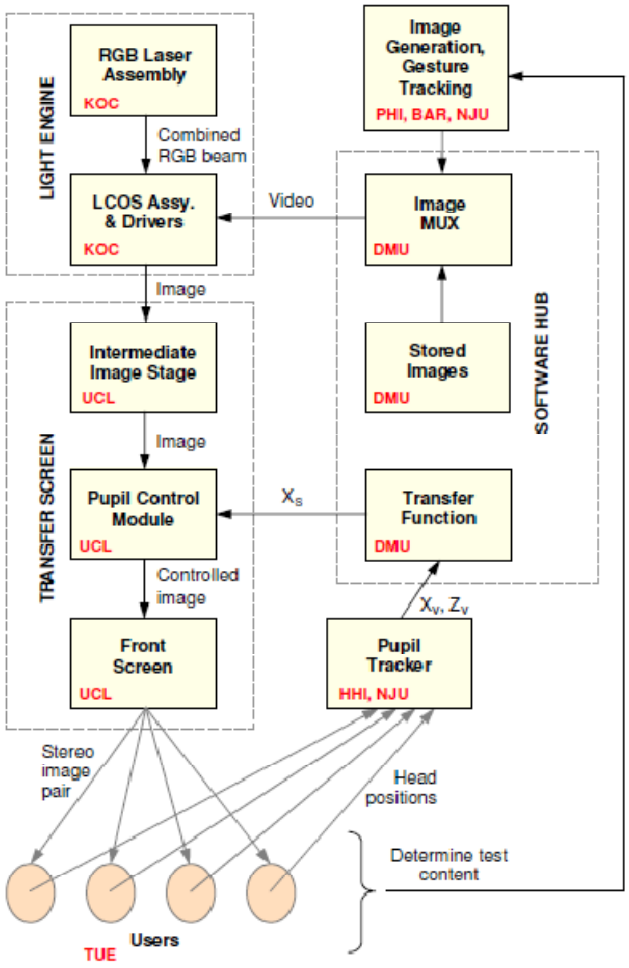

Figure 2.4 Simplified block diagram of the system architecture. The principle partners associated with each area of work is indicated by red

The diagram shows the principal components of the overall display system. The interfaces between the blocks provide natural boundaries with respect to the separate functionalities of the components.

2.3 Functional Blocks

This section includes detailed information about the specifications and the component selections for the different functional blocks of the system. The technological limitations in the blocks and the changes done in the specifications during the project are also given.

2.3.1 RGB Laser Assembly

This thesis will focus on the Light Engine part of the system therefore only brief information will be given about the blocks in the Light Engine in this part of the document. Detailed information including designs, test results and component specifications will be given in the following sections.

The RGB laser assembly provides the illumination source for the display. The input to the system is the interlock where the lasers are cut off in the event of a scanner failure. The lasers used have low etendue (product of source size and solid angle) that enables the high degree of control necessary for this display. The lasers emit continuous and un-modulated beams and as the display has no diffractive components, the high coherence of the light is not exploited.

The output from the beam forming optics will be a narrow vertical column of illumination. The width of this beam will not affect the perceived image quality. However, as the beam gets wider, the depth of available viewer movement in the Z-direction decreases.

2.3.2 LCOS Assembly and Drivers

The LCOS assembly forms and projects an image on the Intermediate Image Stage. The inputs to the assembly are a combined RGB beam, a video signal containing left and right images and sync signal to synchronize the movement of the scanner. The output is 20" diagonal horizontal raster image that is projected at approximately 500 mm distance. The two-dimensional light valve is horizontally scanned with the vertically aligned laser line. The possible candidates for the 2D light valve were FLC (ferroelectric liquid crystal), DMD (digital micro device) and LCOS (liquid crystal on silicon) devices. FLC and DMD devices obtain grey scale by using pulse width modulation and therefore are not suitable for illumination from a scanned illumination source. LCOS devices are analogue and can be used where the illumination on any particular pixel is not continuous. The light engine comprises several principal components which can be listed as:

- Beam shaping optics is required to convert the combined RGB laser beam into the homogenized vertical fan of rays that illuminate the LCOS devices.
- Horizontal scanner is used to provide lateral scanning of the fan of laser rays and scans up to 120 Hz.
- Beam splitting optics is used to guide the red, green and blue beams such that they illuminate the corresponding LCOS devices and the combining optics is used to recombine their outputs.
- 3-channel LCOS and associated drivers are used to create the full-color images.
- Projection lens is required to focus the scanned image columns reflected off the LCOS devices on to the Intermediate Image stage.

2.3.3 Intermediate Image Stage

The intermediate image stage diffuses the real image in the horizontal direction so that the image column fills the entire width of the following stage. The input into this stage is the real projected horizontal raster image from the light engine. The column of the image leaves this stage such that it illuminates the entire SLM width.

L2 is a spherical convex lens that acts as a field lens to concentrate the axes of the diffused light towards the centre of the SLM in the horizontal direction. In the vertical direction, it serves to focus the light coming from the projection lens L1 onto the SLM. A Fresnel lens from Fresnel Optics™ is chosen as L2 and its specifications are given in Table 2.1.

Part Number	Focal Length (mm)	Facet Spacing (mm)	Fresnel Conjugate (mm)	Plano Conjugate (mm)	Clear Aperture (mm)
SC208	279.4	0.508	Infinity	279.4	405.9

Table 2.1 The specifications of the Fresnel lens L2 (from Fresnel Optics™)

The horizontal diffuser must spread the emergent rays from L2 over the width of L3. L3 has a width of 200 mm and it is located 577 mm in front of L3. A diffuser has been located at DMU that spreads the light over a width of 183 mm at a distance of 567 mm. This corresponds to a lenslet with F number of 3.10 in air. Although the spread is slightly less than the diameter of L3, this does not matter as the outer regions of this lens are unusable due to excessive spherical aberration. The lens pitch of this screen is 0.385 mm with a radius of 0.72 mm and the thickness is 1.18 mm. The pitch of the array is larger than the size of the pixels imaged onto L2 which may causes cases where a pixel may be imaged by the part between the two adjacent micro-lenses. This may cause gaps or dark

vertical bands appearing in the final image. The case where the pitch of the micro-lens is larger than the size of the pixel image, resulting in non-uniform diffusion, is shown in Figure 2.5 The figure illustrates the case where the pitch of the microlens array is larger than the size of the pixel image. The beams that hit the intersection araeas of the micro-The six adjacent pixels (shown with different colors) imaged onto L2, passes through the lenticular horizontal diffuser (D1). The beams that hit the regions between the micro-lenses spread around and cause non-uniform diffusion of the light.

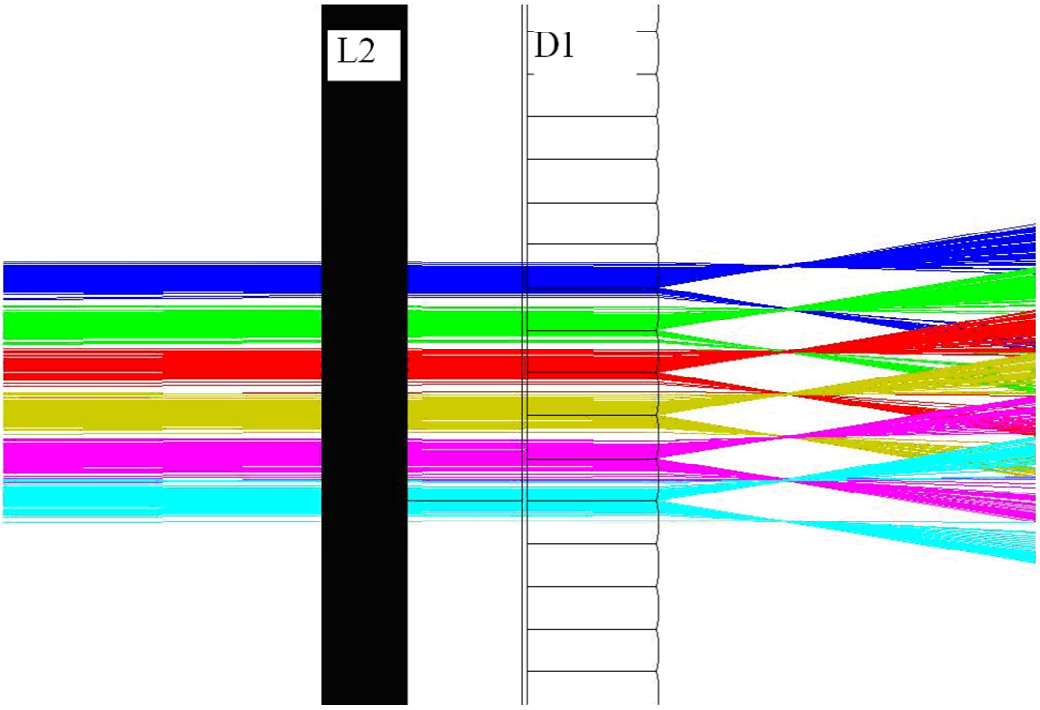

Figure 2.5 The figure illustrates the case where the pitch of the microlens array is larger than the size of the pixel image. The beams that hit the intersection araeas of the micro-lenses spread around and cause non-uniform diffusion

2.3.4 Pupil Control Module

The Pupil Control Module controls the directions of the beams exiting the front screen and projects the image on the Intermediate Image Stage. This module includes a spherical convex lens L3 and a linear SLM having switchable vertical apertures. The light from the previous section is concentrated onto the lens L3 and the input from the Transfer Function module determines the locations of the openings on the SLM. The front screen is located at the Fourier plane of the SLM therefore the pattern on the SLM is transformed into exit pupils in the viewing field without being imaged by the system.

In the first prototype a large plano-convex lens at DMU is used and its parameters were measured by DMU. The results of the measurements of the lens are given in Table 2.2. Single lenses perform poorly at imaging over wide angles due to field curvature so compound lenses consisting of several elements is planned to be used in the second prototype of the Transfer Screen. Different alternatives have been analyzed by UCL and the performance of the triplet lens is found to be superior to other options such as bi-convex spherical lens, meniscus lens and aspheric lens.

Refractive Index	Surface ROC (mm)	Diameter (mm)	Edge Thickness (mm)	Center Thickness (mm)
1.532-1.567	178.55	200	4.4	35

Table 2.2 The specifications of the plano-convex spherical lens L3

The SLM must be fast in order to cope with the exit pupils that are furthest from the conjugate plane of the SLM in the viewing field. As it has been explained before, in order to create dynamic exit pupils, the aperture must move position over the duration of the horizontal scan. Therefore, the speed of SLM limits the number of viewers that the display system can support. SLM needs to be continuous as any breaks will give the appearance of

vertical dark bands. The dimensions of the SLM has to be big enough (25 cm width) and it has to have sufficient pixels to select the exit pupil without cross talk. The number of required pixels depends on the cross talk at different viewing positions and the properties of the superlens transfer screen. According to UCL's ray-tracing results a resolution of 512 pixels (resulting in a minimum aperture of 0.39 mm) in the horizontal direction is sufficient to enable the exit pupil to be moved across the viewing field in increments that are small in relation to the eye spacing.

2.3.5 Front Screen

The Front Screen assembly magnifies the input angle that has been determined by the SLM to provide an acceptable wide viewing angle. The horizontally scanned image from the Pupil Control module (where the rays from certain directions have been blocked) enters the screen and the light from each image column goes to the specific eyes of the viewers. The Front Screen consists of four components that can be seen in Figure 2.6.

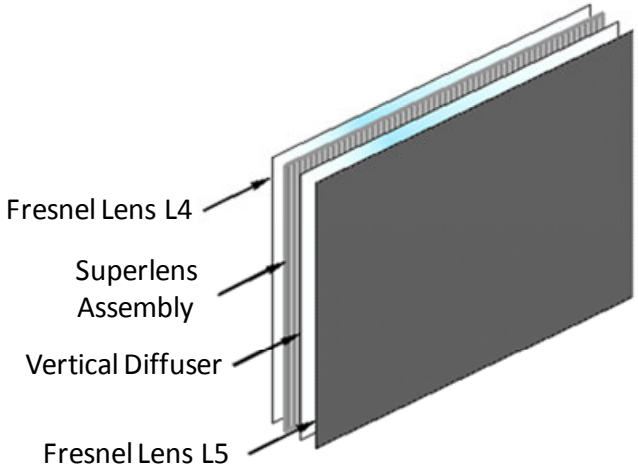

Figure 2.6 The schematic of the components of the Front Screen

L4 is an aspherical Fresnel lens and it collimates the diverging rays from the SLM such that their axes enter the superlens assembly orthogonally to its surface. A Fresnel lens from Fresnel Optics™ is chosen as L4 and its specifications can be seen in Table 2.3. It has a rather large facet spacing of 0.508 mm but it is observed that when this lens is placed adjacent to a 45 lines per pitch (LPI) lenticular screen and the separation between L4 and the superlens assembly is bigger than 15 mm, Moiré fringing is not particularly noticeable over the majority of the screen.

Part Number	**Focal Length (mm)**	**Facet Spacing (mm)**	**Fresnel Conjugate (mm)**	**Plano Conjugate (mm)**	**Clear Aperture (mm)**
SC213-600	762	0.508	Infinity	762	600x590

Table 2.3 The specifications of Fresnel lens L4 (from Fresnel Optics™)

The superlens assembly is a one dimensional version of a Gabor Superlens. Superlenses are collections of micro-lens arrays that behave as a much larger optical system than the individual lenticules [65]. The cylindrical micro-lens arrays used in the superlens assembly have equal pitch but have different focal lengths. The superlens screen of the system additionally magnifies the input angle by a factor M in the horizontal plane thus increasing the width of the viewing field of the display. As it is shown in Figure 2.7, a reversed Keplerian layout including a field lens array is used in the Front Screen.

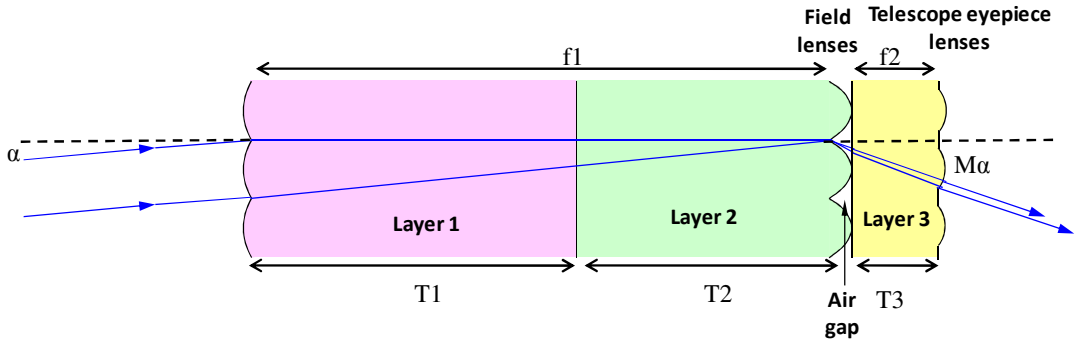

Figure 2.7 Side view of superlens screen with three layer Gabor superlens. The incidence angle is magnified by a factor of M by the system

The superlens screen consists of three layers of cylindrical micro-lens arrays. The first layer is an objective lens and it focuses the beam in the second layer. The second layer is a field lens changes the direction of the passing through it. The third layer is an eyepiece lens and it collimates the transmitted light. If the incident angle exceeds a certain value, the beams that have passed through the first layer escape to the neighboring lenticule in the second layer resulting in undesired output beam angles. The magnification M of the superlens screen is roughly equal to the ratio of the focal lengths of the first layer (f1) to the second layer (f2). The value of f1 is equal to the sum of the thickness of the first two layers (T1 and T2) and f2 is equal to third layer thickness T3. In order to maximize the magnification, T3 should be chosen small compared to the sum of T1 and T2.

The vertical diffuser expands the beam vertically in order to provide freedom of movement in the vertical direction. This diffuser must be located close to the superlens screen to minimize blurring of the image. The horizontal diffuser's specifications are also compatible with the specifications of the vertical diffuser; therefore the same diffuser will be used in the Front Screen.

L5 is an aspherical Fresnel lens and it focuses the beam at two meters in the horizontal plane to achieve the desired viewing field and two meters in the vertical direction in order to concentrate light to the region where the viewers are located. The focal length of L5, determines the range of viewing distances from the front screen. As the focal length gets shorter the viewers can be located closer to the display and vice versa. A search of suppliers has not revealed a source for a lens with such a long focal length. In order to avoid the necessity of having a custom-built lens, a Fresnel lens from Fresnel Optics™ is chosen as L5 and its focal length is modified by using a liquid layer in contact with the faceted face of the lens. The specifications of L5 can be seen in Table 2.4.

Part Number	Focal Length (mm)	Facet Spacing (mm)	Fresnel Conjugate (mm)	Plano Conjugate (mm)	Clear Aperture (mm)
SC214	609.6	0.508	Infinity	609.6	462.1

Table 2.4 The specifications of Fresnel lens L5 (from Fresnel Optics™)

If the focal length of L5 in air is F_A and the refractive indices of L5 and the liquid are N_F and N_L respectively, the focal length of L5 with liquid in contact F_L can be found as:

$$F_L = F_A\left(\frac{N_F - 1}{N_F - N_L}\right) \quad (2\text{-}1)$$

2.3.6 Pupil Tracker

The pupil tracker provides the positional information of the eye pupils of the viewers to the system. The images captured by a camera array are used to determine the positions of the viewers and the coordinates in the X, Y and Z plane is sent to the Transfer Function module.

The Pupil Tracker can provide the head position coordinates to a precision that enables the images to be rendered in accordance with viewer position thus permitting the presentation of motion parallax. The accuracy of the system also increases the perceived brightness by increasing the precision of the beam direction and decreases the crosstalk caused by any beam misdirection.

2.3.7 Software Hub

The eye pupil coordinates of the viewers, computer generated (CG) video and scanner position enter the Software Hub and it manages the laser safety interlock, image multiplexing, image storage, scanner driver, transfer function, SLM shift register and synchronizes all functions.

The laser safety interlock is needed in the case of a scanner failure where a potential damage to viewers' eyes can occur. The scanner failure sensing is done by using the closed loop signal coming from the used galvanometer scanner. The closed loop control of the scanner will also be used to control the scanner driver.

The primary focus of the first prototype is in temporal MUX stereo images. The video card will be driven by a video stream for the left and the right channels and alternate fields from left and right will be temporally interleaved.

The images in the first prototype are synchronized by the signals from the Master Sync module and are stored in the PC. The transfer function calculates the dynamic aperture region of the SLM in the case where the exit pupil is not in the conjugate plane of the SLM. The Master Sync allows the 3D image formation by synchronizing the images, the scanner and the SLM.

3 FUNCTIONAL PARTS OF THE LIGHT ENGINE

The Light Engine includes different functional parts including RGB lasers, laser beam combining optic, laser beam shaping and homogenizing optics, the scanner, the LCOS unit and the projection lens. The component selection for different functional parts and the specifications and the characterization methods of the selected components will be given in this section.

3.1 RGB Laser Unit

The availability of efficient, small, cheap lasers that can emit high power laser beam in the visible wavelength range triggered the recent developments in the laser based displays. An immediate advantage of using spectrally pure laser light for displays is the wide color gamut that they can produce which can be seen in Figure 3.1. There are many different types of lasers available but when they are evaluated with respect to their weight, volume, cost and efficiency, laser diodes are better candidates for the display technologies [66].

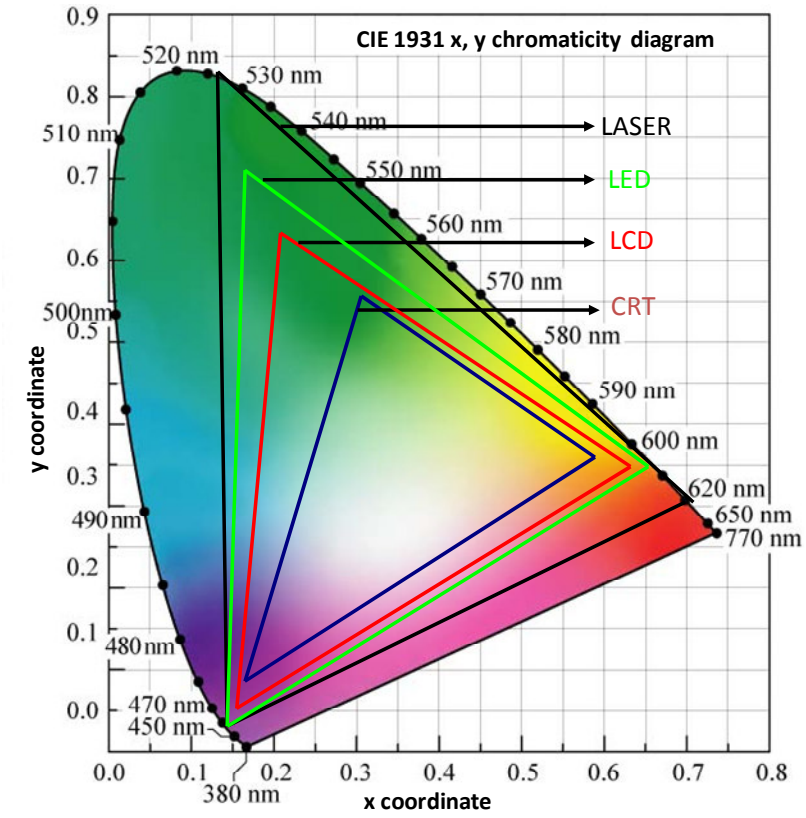

Figure 3.1 1931 CIE x,yY choromaticity diagram showing the color gamut that can be obtained with different display technologies

The first semiconductor laser based on GaAs was invented in 1962 [67-69]. The first devices required cryogenic temperatures and they were operated in pulsed mode. Continuous wave (CW) operation at room temperature was later demonstrated with a hetero-junction approach which gave rise to an efficient confinement of carriers and photons to the active region of the device [70, 71].

Many display applications require high output optical power (portable displays require low optical power) and good beam quality but the conventional semiconductors are unable to meet both at the same time. Vertical cavity surface emitting lasers (VCSELs) use a

surface emitting structure in contrast to the edge emitting conventional diodes and provide a better beam quality. The output power of diodes are limited (in the order of a few hundred milliwatts) but can be increased by stacking diodes together. The first VCSEL type laser diode was introduced in 1979 [72]. The typical architecture of a surface emitting diode and its output beam profile are shown in Figure 3.2.

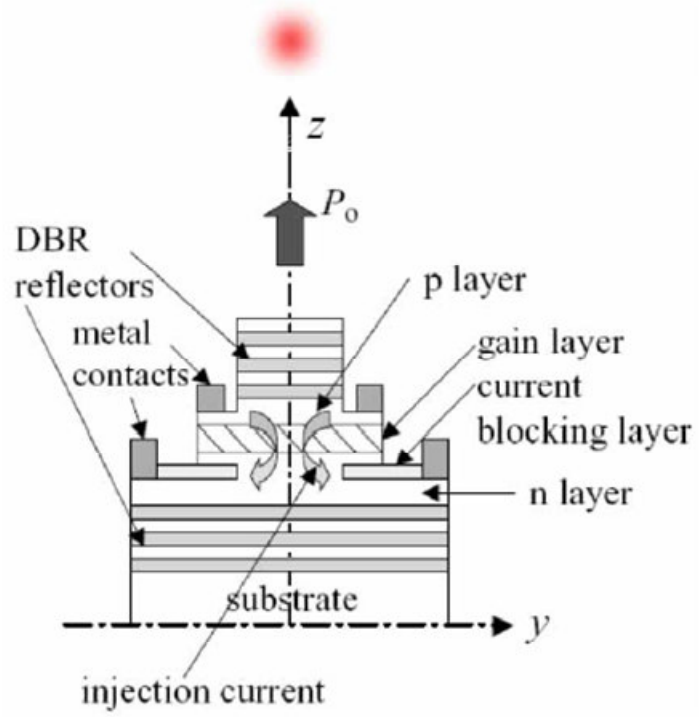

Figure 3.2 The structure of a typical VCSEL. The laser has a circular output beam profile [73]

The RGB laser unit in Helium3D includes red, green and blue lasers and the beams from the three lasers are combined to form a white output as illustrated in Figure 3.3. The figure shows a simplified version of the beam shaping and combining optics. The specifications of the chosen lasers are critical as they will directly determine the output

image quality. Therefore, lasers from many different laser companies have been searched before making a selection. The critical parameters that were checked for selecting the lasers are:

- Low coherence length to reduce the speckle formation at the output
- Sufficient power to meet the brightness specifications (at least 50 foot Lamberts)
- Appropriate wavelengths for producing a large color gamut
- Affordability within the given project budget

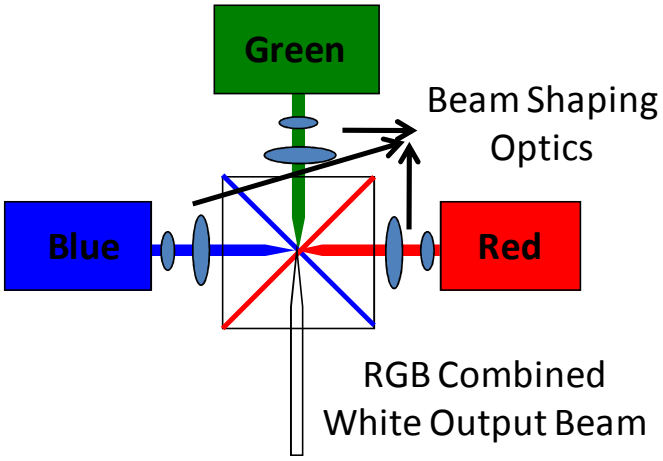

Figure 3.3 Simplified schematic of the RGB laser unit in the Light Engine

3.1.1 Single Emitter Lasers

Two different prototypes of the Light Engine were designed during the project period. In order to check the compatibility of the LCOS unit with the laser scanning illumination and to control the system for any unexpected image artifacts, low power (in the order of a few hundred milliwatts) single emitter laser diodes were used in the first prototype. There was no commercial single emitter red laser with the required specifications; therefore a laser with four emitters was chosen and a line was created from its two emitters. The

specifications of the red, green and blue lasers used in the first prototype are given in Table 3.1, Table 3.2 and Table 3.3 respectively. The calculated total output luminance with these lasers is 8.1 ft-L.

Red Laser (from Syncrovision™)	
Product Number	600-r-KV
Wavelength	640nm
Output Power	600mW
Beam Diameter	3mm
Beam Divergence	0.8mrad (full angle)
Operating Mode	CW
Transverse Mode	TEM_{00}
Number of emitters	4 (2x2 array)

Table 3.1 Specifications of the red laser used in the first prototype

Green Laser (from Laser 2000™)	
Product Number	MGL-III-532
Wavelength	532nm
Output Power	300mW
Beam Diameter	2mm
Beam Divergence	1.5mrad (full angle)
Operating Mode	CW
Transverse Mode	TEM_{00}
Number of emitters	1

Table 3.2 Specifications of the green laser used in the first prototype

Blue Laser (from Laser 2000™)	
Product Number	MBL-III-473
Wavelength	473nm
Output Power	200mW
Beam Diameter	2mm
Beam Divergence	1.5mrad (full angle)
Operating Mode	CW
Transverse Mode	TEM_{00}
Number of emitters	1

Table 3.3 Specifications of the blue laser used in the first prototype

3.1.2 Power Ratio Calculation and White Balancing

Selection of the primary wavelengths for additive mixing and the required optical powers for these wavelengths, depend on the response of the human visual system at the respective wavelengths. The power ratio between the individual lasers needs to be calculated and adjusted carefully so that the output images do not have a dominant color or other color mismatches.

The human eye has two types of photoreceptors which are called rod and cone photoreceptors. The cone receptors are sensitive to medium and high brightness color vision, with sensitivity peaks in short (420–440 nm), middle (530–540 nm), and long (560–580 nm) wavelengths which correspond to primary colors [74]. The tristimulus values of a color are denoted by X, Y, and Z and they are the amounts of three primary colors in a three-component additive color model [75]. A color space is a method for associating tristimulus values with each color. In order to determine the perceived color of the displayed images in Helium3D, CIE 1931 XYZ color space created by the International Commission on Illumination (CIE) in 1931 [76] was used. The color space was found by combining the specifications of the CIE RGB color space with the results of a series of experiments and is commonly used as a standard. The procedures adopted during the

experiments and the calculations can be found in the literature [77]. The CIE 1931 XYZ color matching functions calculated for the three colors are shown in Figure 3.4.

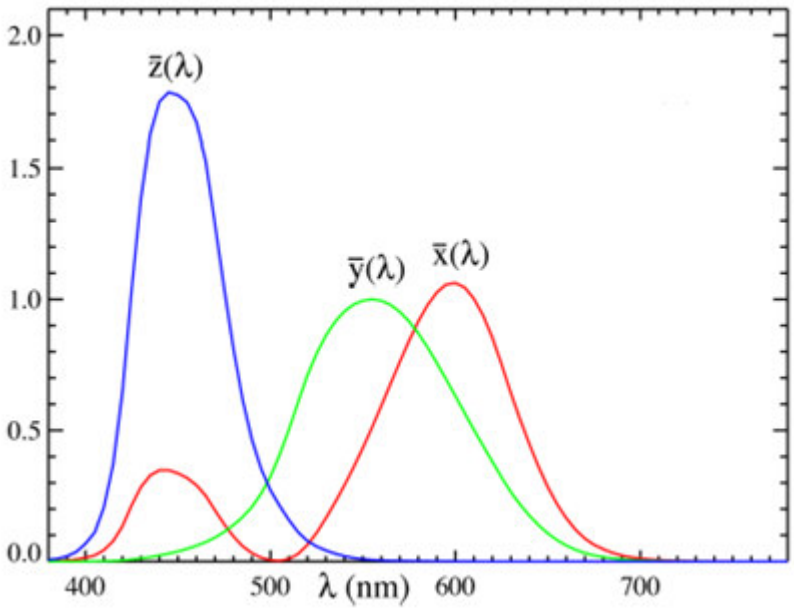

Figure 3.4 The plot of the 1931 CIE XYZ color matching functions. Unlike RGB color space, the weight factors in the XYZ color space are always positive [66]

Color matching functions are the calculated weight factors during the experiments and they make it possible to calculate the XYZ coordinates for an arbitrary spectral power distribution P(λ) by using the equations below where k is a normalization constant [78].

$$X = k \int P(\lambda)\,\bar{x}(\lambda)\,d\lambda \tag{3-1}$$

$$Y = k \int P(\lambda)\,\bar{y}(\lambda)\,d\lambda \tag{3-2}$$

$$Z = k \int P(\lambda)\,\bar{z}(\lambda)\,d\lambda \tag{3-3}$$

The diagram in Figure 3.1 is a two dimensional 1931 xyY CIE chromaticity diagram and it is obtained by a special projection of the three dimensional CIE XYZ color space. The monochromatic wavelengths are located at the outer border of the chart and the diagram represents the color gamut of the human visual system.

The relative luminance of the primaries is decided based on the display's white point. The designated coordinates of the white point by ITU-R BT.709 standard is (0.3127, 0.3291). It is possible to determine the relative optical powers required for this white point if the color coordinates of the primaries are known [79]. Alternatively the required optical power of three primaries with specified wavelengths R(λ1), G(λ2) and B(λ3) for a specified color temperature can be evaluated if the tristimulus values X and Z are known (Y is normalized to 100). The following matrix operation can be performed to evaluate the required optical power.

$$\begin{bmatrix} \bar{x}(\lambda_1) & \bar{x}(\lambda_2) & \bar{x}(\lambda_3) \\ \bar{y}(\lambda_1) & \bar{y}(\lambda_1) & \bar{y}(\lambda_1) \\ \bar{z}(\lambda_1) & \bar{z}(\lambda_1) & \bar{z}(\lambda_1) \end{bmatrix} -1 \begin{bmatrix} X \\ Y \\ Z \end{bmatrix} = k \begin{bmatrix} P(\lambda_1) \\ P(\lambda_2) \\ P(\lambda_3) \end{bmatrix} \quad (3\text{-}4)$$

For a laser based display, calculations are needed to determine the power levels of red, green and blue lasers required for a white output. The accepted color temperature standard for displays is 6500K denoted as D65. The XYZ chromaticity co-ordinates for this color temperature are X = 95.017, Y = 100 and Z = 108.813. The values of the color matching functions of the specified wavelengths can be found in special color books [80].

If one tries to obtain 6500 K white light from three laser wavelengths, the optical power ratio depends on the wavelengths chosen. A display system produced with lasers with specified wavelengths will be able to reproduce the colors enclosed in the triangular region obtained by connecting these primary wavelengths in the chromaticity diagram. It can be

immediately seen that displays with three primaries are unable to reproduce all colors perceivable by the human visual system. Instead of using three primary wavelengths, one can use four or more primary wavelengths for an enhanced color gamut at the expense of increased design complexity and cost. The methods for achieving a desired white point in these multi-primary displays are described in the literature [81, 82].

The power levels of red, green and blue lasers required for creating a white output at 6500K have been calculated in MATLAB™ with the help of Dr. Kishore V.C. The power ratios acquired by using the specifications of the low power lasers used in the first prototype is shown in Table 3.4. The system is blue limited therefore some of the optical power of the red and the green lasers is thrown away. As explained before a laser with four emitters was used in the first prototype. The laser's emitters were a two by two array; therefore its two emitters were switched off in order to create a single line. The maximum optical power of the red laser dropped to half but since the system was blue limited, the total optical power decreased by only 5% (from 673mW to 638mW).

	Red	Green	Blue
Power (mW)	**600**	**300**	**200**
Wavelength (nm)	640	532	473
Calculated Power Ratio	1,58	0,78	1,00
Required power	316,56	156,58	200,00
Excess power from each color	283,44	143,42	0,00

Table 3.4 Power ratio calculation for the first prototype. The system is blue limited

3.1.3 Lasers with Multiple Emitters

The second prototype is the final version of the display system therefore; it needs to provide a satisfying output luminance. The minimum requirement from a CRT television in a well-lit room viewing condition is 50 foot-lamberts and this value drops to 16 foot-

lamberts in dark room viewing conditions. In order to produce a luminance above 50 foot-lamberts, lasers with optical output power in the order of a few Watts have been searched.

After taking the parameters explained before into consideration, the lasers from Necsel™ have been found suitable as they offer high power and low coherence length. The specifications of the chosen lasers for the second prototype are given in the tables below. Approximately 80% of the color range that a human can perceive and a predicted 85.4 foot-lambert output luminance can be produced by using the selected lasers.

Red Laser (from Necsel™)	
Product Number	NECSEL-640-5000
Wavelength	640nm
Spectral Width at FWHM	3nm
Output Power	5W
Emitting Area Width	40µm
Emitting Area Period	200µm
Beam Divergence (full angle)	Slow axis 7° Fast axis 40°
Operating Mode	CW
Transverse Mode	TEM_{00}
Number of Emitters	20 (20x1 array)

Table 3.5 Specifications of the red laser chosen for the second prototype

Green Laser (from Necsel™)	
Product Number	NECSEL-532-3000
Wavelength	532nm
Spectral Width at FWHM	0.2nm
Output Power	3W
Beam Diameter at FWE2	0.08mm
Emitter Intra-row Spacing	0.32 mm
Beam Waist Location	-14.5 mm (row1), -30mm (row2)
Beam Divergence (full angle)	10mrad
Operating Mode	CW
Transverse Mode	TEM_{00}
Number of Emitters	48 (24x2 array)

Table 3.6 Specifications of the gree laser chosen for the second prototype

Blue Laser (from Necsel™)	
Product Number	NECSEL-465-3000
Wavelength	465nm
Spectral Width at FWHM	0.2nm
Output Power	3W
Beam Diameter at FWE2	0.08mm
Emitter Intra-row Spacing	0.32 mm
Beam Waist Location	-14.5 mm (row1), -30mm (row2)
Beam Divergence (full angle)	10mrad
Operating Mode	CW
Transverse Mode	TEM_{00}
Number of Emitters	48 (24x2 array)

Table 3.7 Specifications of the blue laser chosen for the second prototype

As it can be seen from the specifications of the chosen lasers, the red laser is very different compared to the green and the blue lasers. The differences in the beam divergence, beam size and the number of emitters increase the difficulty of combining their

output to create a homogenized white light. The power ratio calculation results obtained by using Necsel™ lasers are given in Table 3.8. The system was supposed to be red limited but the double column configuration of the green and the blue lasers prevent the use of the full optical power. Different methods for using the both columns have been studied but due to the limited volume between lasers and the beam shaping optics and the complexity of the solutions, those methods haven't been applied. Using single column decreased the maximum total optical power by 39% (from 10.37W to 6.35W) but the output luminance is still in the acceptable range (85.4 foot-lambert).

	Red	**Green**	**Blue**
Power (mw)	**5000**	**1750**	**1750**
Wavelength (nm)	640	532	465
Calculated Power Ratio	1,75	1,00	0,88
Required power	3069,50	1750,00	1534,75
Excess power from each color	1930,50	0,00	215,25

Table 3.8 Power ratio calculation for the second prototype. The system is green limited

3.2 Laser Beam Combining Optics

The next functional unit in the Light Engine is the laser beam combining unit. Different approaches for combining the three laser beams have been studied and their advantages and disadvantages have been analyzed. The three solutions that were pursuit are the waveguide combiner option, the fiber coupling option and the free space option.

3.2.1 Waveguide Combiner Option

The advantages of this method are its independence from the input frequency due to the material used (polymer is transparent in the visible frequency range) and the flexibility that it can provide in coupling the laser to the waveguide. On the other hand, the waveguide

combiner option is very challenging since there are no off the shelf waveguides with 100 micrometer or less thickness therefore; this approach requires a new design and fabrication process. Due to limitations in time, cost and expertise in the specific area this approach has not been followed.

3.2.2 Fiber Coupling Option

In this case, the output of each laser is coupled to a single fiber and then combined together. The Necsel™ lasers have multiple emitters therefore they require special optics to be coupled to a fiber. A method of combining multiple emitters into a single fiber is illustrated in.

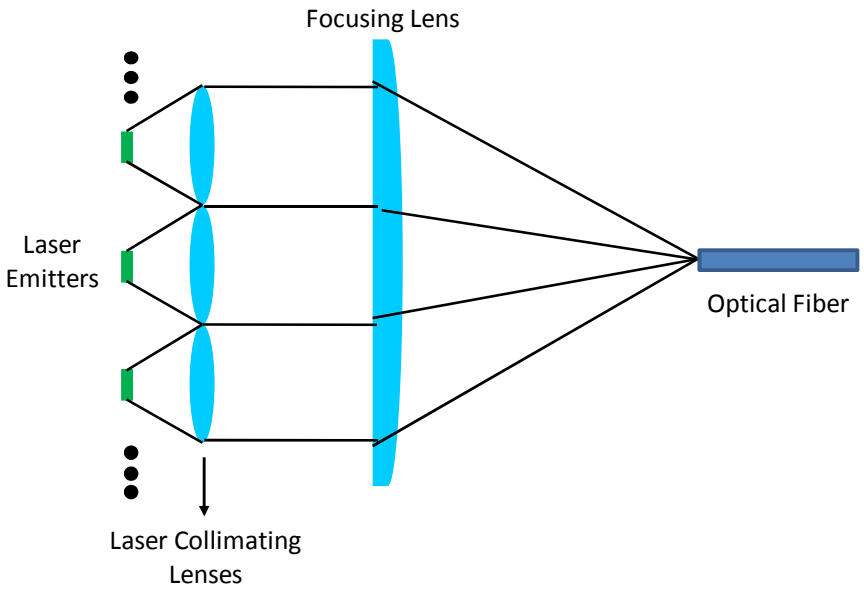

Figure 3.5 Coupling of a laser with multiple emitters to an optical fiber. A micro-lens array is used to collimate the output of multiple emitters and a focusing lens is used to focus the combined beam into a fiber [83]

During the project, different off-the-shelf fibers were found and their properties have been analyzed. One of the important parameters that needed attention was the working wavelengths of the chosen fibers. The mismatch between the fiber and the laser beam causes loss in the system. The commercially available fibers' working wavelengths were not perfectly matching with the second prototype's specifications (for the red and the blue lasers).

A fiber coupler for the Necsel laser has been designed in ZEMAX™ and the coupling efficiency has been calculated. Fiber core radius was varied from 0.03mm to 1mm in the design and the corresponding efficiencies were analyzed at various field points. According to the results, even in the best fiber radius selection scenario (when the radius is 0.03mm), the coupling efficiency ranges from 86% for the middle emitter to 50% for the emitter at the edge (at 3.84mm from the center). The design was assuming a perfect alignment and the use of a lens group composed of three lenses for focusing the beam into the fiber. This approach would have required the fabrication of special lenses and a very critical alignment; therefore it has not been pursuit. Another reason for not using fiber coupling option is the requirement of additional optics for collecting and expanding the beam coming out of a fiber. Detailed information about the modeling of a fiber coupler and the calculation of coupling efficiency in ZEMAX can be found in the following section.

3.2.3 Free Space Option

In this approach, the outputs of the lasers are processed directly by the optical components. The beamlets from the lasers are shaped using appropriate optics to have a size around 15 mm in the vertical direction. After controlling the divergence and size of the R, G and B beams, they will be sent to an X-cube for combining. This approach was adapted for its simplicity and efficiency. The required beam shaping optics for this

approach was designed and it was implemented in the first prototype. An X-cube was taken off from an old commercial projector and was used in the set up. The X-cube has a clear aperture of 15mm x 18mm and the measured the transmission spectrum of the cube is given in Figure 3.6. In order to make the measurement an incandescent lamp has been used as input and its spectrum was measured. Then, the spectrum of the exiting beams were measured and normalized according to the reference input beam. The wavelengths of the lasers used in the first prototype were within the transmission spectrum of the X-cube, therefore no other commercial X-cubes have been purchased.

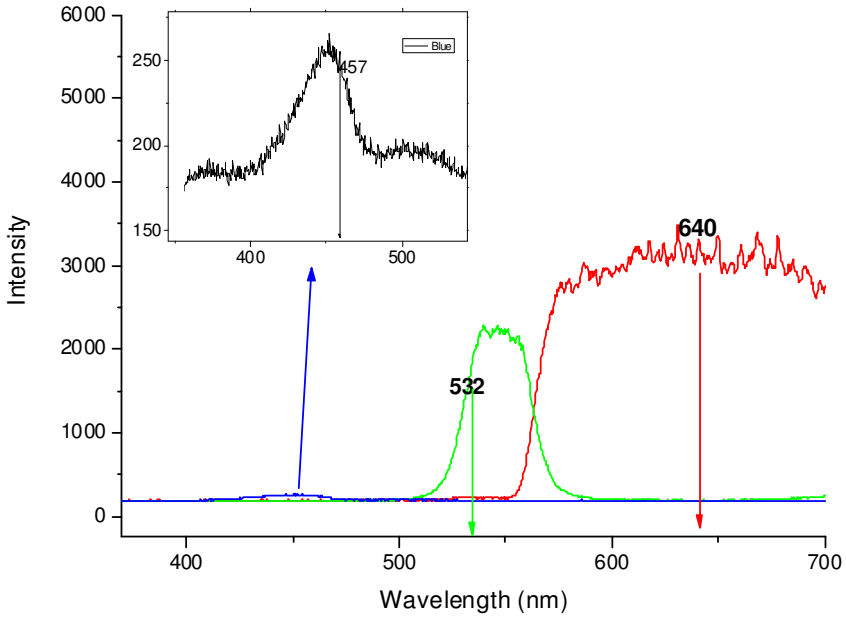

Figure 3.6 The measured transmission spectrum of the X-cube used in the first prototype

3.3 Laser Beam Shaping Optics

The laser beam shaping unit adjusts the size and the angle of the beams from the lasers and homogenizes the output to create a uniform illumination. In order to use in the first prototype, commercially available Gaussian to top-hat convertors have been searched. Most of the convertors require a collimated input coming from a single emitter and the uniform illumination is achieved at a single plane. The lasers of the second prototype have multi emitters and the laser line is needed to stay homogenized for some distance; therefore beam convertors were not acquired for the first prototype to avoid unnecessary cost. The first prototype was built without using any homogenizers, but a fly's eye beam homogenizer is designed for the second prototype.

3.3.1 Beam Shaping of Single Emitter Lasers

The beam shaping and combining of the RGB lasers in the first prototype is illustrated in Figure 3.7. The laser beams combined with an X-cube are sent to a beam expander in order to increase the beam diameter to 11mm. The expander is a commercial 5X beam expander from Thorlabs™. Then the expanded light passes through a cylindrical lens with 150mm focal length to create a line and the output beam is scanned over the LCOS unit with the help of a scanner. In this configuration, an aperture can be inserted after the beam expander in order to control the size of the line length but due to diffraction effects that can be caused by an aperture and the power loss, it is better to adjust the line length with the beam expansion ratio. The laser line formed with this configuration does not provide a uniform illumination but it was used to test the working principle of the light engine, to check the compatibility of the LCOS module with laser line scanning illumination and to measure the system efficiency experimentally.

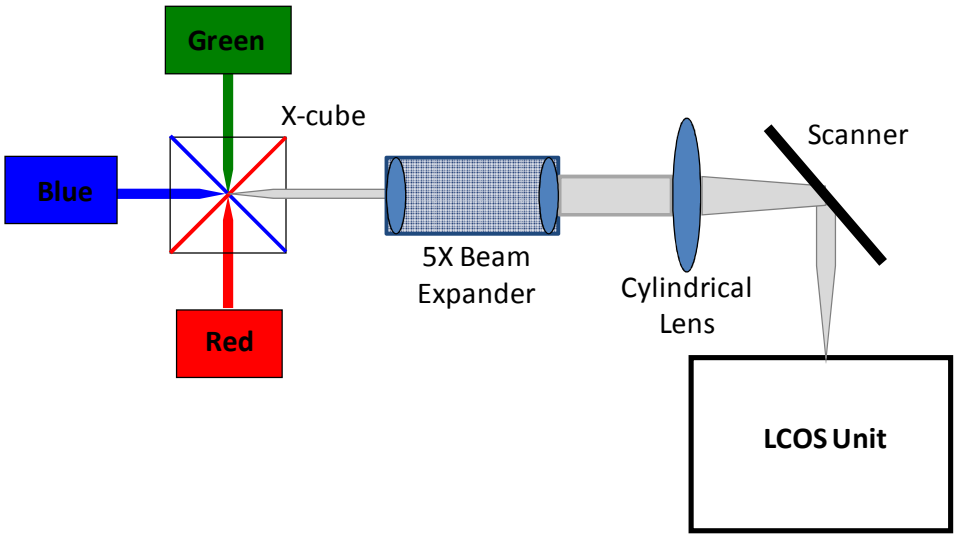

Figure 3.7 Illustration of the beam shaping and combining optics of single emitter RGB lasers used in the first prototype

3.3.2 Beam Shaping of Multi Emitter Lasers

The beam shaping of lasers with multiple emitters is a challenging task compared to shaping single emitter lasers. After passing through different optical elements, beams from individual emitters can separate and cause non uniform illumination and loss of light. The micro-lens based solution for shaping and homogenizing lasers with multiple emitters is illustrated in Figure 3.8. The optical configuration is known as “fly’s eye configuration” because of its similarity to the multiple lens structure of a fly’s eye.

The laser lenslet array controls the divergence angle of the output beams and with the help of the first field lens (FL1), the beams from all the emitters are expanded and overlapped onto the second filed lens (FL2). FL2 collimates the incoming beam so that the overlapped beams enter the uniformizer lenslet arrays as a collimated single beam. The second section of the system works as a regular beam homogenizer that accepts a single

collimated beam. The two uniformizer lenslet arrays have the same specifications and are located one focal length apart from each other. They divide the input beam into smaller parts and mix them together. The remaining field lenses (FL3 and FL4) collect the beams from the uniformizer lenslet array and collimate the output beam. The focal lengths of FL3 and FL4 determine the size of the output beam. All the field lenses in the design are cylindrical lenses and the micro-lens arrays are lenticular lenses. The final focusing lens is also a cylindrical lens but it is rotated 90° with respect to others. It focuses the beam in the axis perpendicular to the emitters to create a thin line.

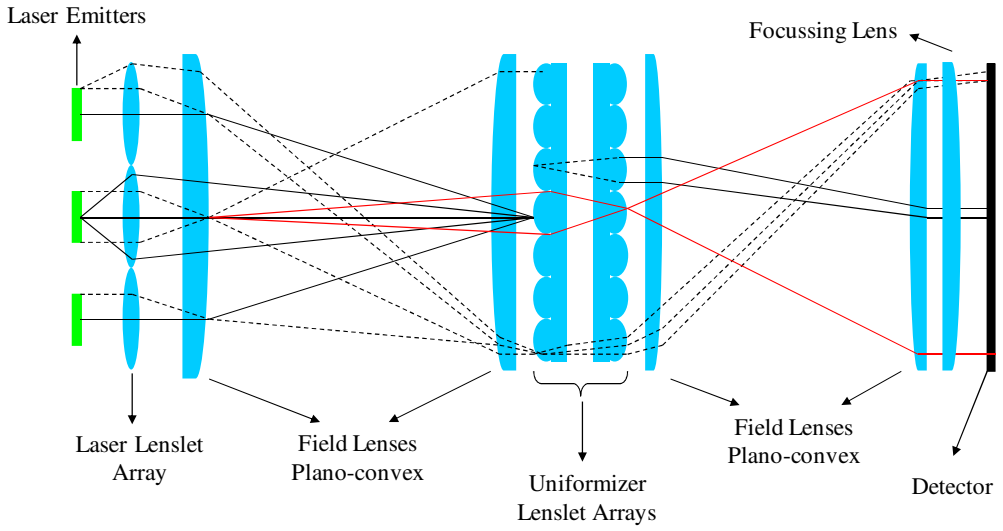

Figure 3.8 Optical layout of the fly's eye laser array homogenizer [84]

If all the lenses (including the micro-lens arrays) are replaced with spherical lenses, the beam is homogenized in both axes. This is not needed for the Light Engine because the laser line is scanned along the axis perpendicular to the line and the overall intensity is averaged by the human eye. Using spherical lenses increases the alignment difficulty by introducing a new axis; therefore it is unnecessary. On the other hand, a non-uniform

illumination along the laser line causes intensity variations at the displayed images that can be easily noticed by the viewer. The laser beam shaping optics for three colors including beam homogenizer is shown in Figure 3.9.

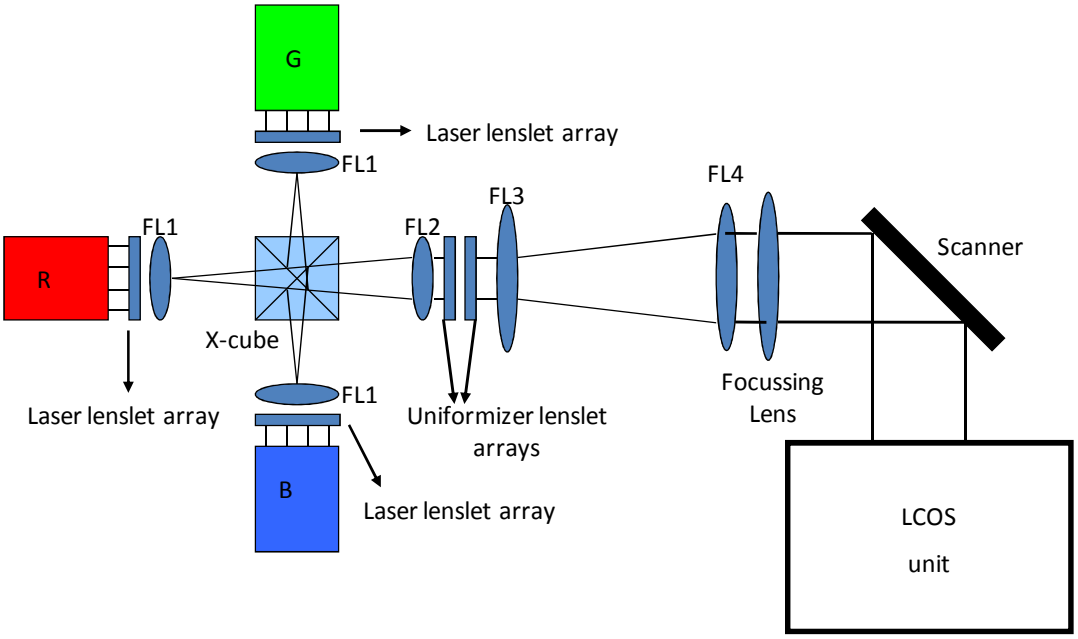

Figure 3.9 Illustration of the beam shaping, combining and homogenizing optics of multi emitter RGB lasers

3.3.3 Laser Illumination Column Width

The laser beam shaping optics creates a uniform laser line that is scanned over the LCOS unit. The effect of the laser column width that scans the LCOS (H) can be determined by considering the overall magnification B between the LCOS and the front screen and then applying the projected column width to the geometry of the screen. The overall magnification can be found by dividing the screen width with the active LCOS width. Then by referring to Figure 3.10, B times H gives the laser line width on the screen. D is the viewers distance from the screen and N is the focal length of the final lens in the

front screen (L5). K can be considered as effectively being the PSF width of the SLM. This value can be added to the other factors contributing to crosstalk such as SLM response time, superlens diffraction, scattering etc.

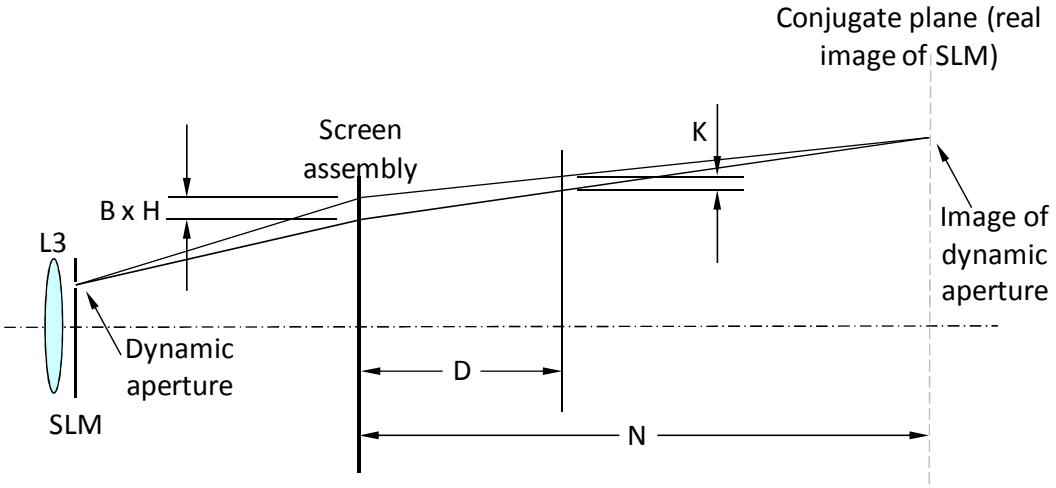

Figure 3.10 Illustration of the laser illumination column width effect on the exit pupil size

From the similar triangles:

$$\frac{K}{N-D} = \frac{B*H}{N} \tag{3-5}$$

Solving for K results in:

$$K = (B*H)*\frac{N-D}{N} \tag{3-6}$$

For a 20” diagonal screen and a 0.7” diagonal LCOS unit, the magnification B is equal to 28.57. If the scanned beam is 0.1mm wide and the focal length of L5 is 2000mm, then at a 500mm viewing distance K is equal to 2.14mm. Even if the beam width is much larger

than the LCOS pixel width, as long as the values of K are small compared to the interocular distance the system works without crosstalk.

3.4 The Scanner

The scanner is used to provide horizontal scanning of the combined laser line on to the LCOS unit of the display. A closed-loop controlled system that can be driven with ramp scan waveform up to 120 Hz (for single viewer) is required. A galvanometric scanner from General Scanning™ is acquired with its driver and used in the first prototype of the system. The same scanner is planned to be used in the prototype of the system. The size of the scanner and the mirror is shown in Figure 3.11 and the specifications of the scanner can be found in Table 3.9.

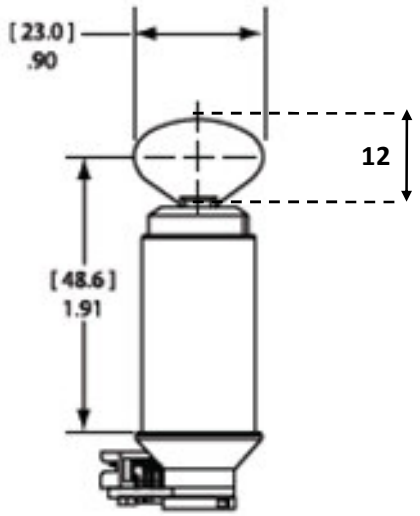

Figure 3.11 Schematic of the scanner and the mirror from General Scanning™ (values are in mm)

Galvanometric Scanner (from General Scanning™)	
Product Number	VM2500+
Driver Model	MiniSAX II
Mirror Size	12mm x 23 mm
Maximum Scan Angle	±40° (optical)
Maximum non-linearity	0.2 % (for ±20° optical)
Retrace time	1.68ms (at 120Hz with ±4°)

Table 3.9 Light Engine scanner specifications from General Scanning™

3.5 The LCOS Unit

The LCOS unit is composed of three LCOS chips as illustrated in Figure 3.12. The white light enters the LCOS unit and it is separated into red, green and blue colors by the filters. Each color illuminates the specific LCOS chip and the modulated light reflects back. The reflected beams are combined together and leave the LCOS unit.

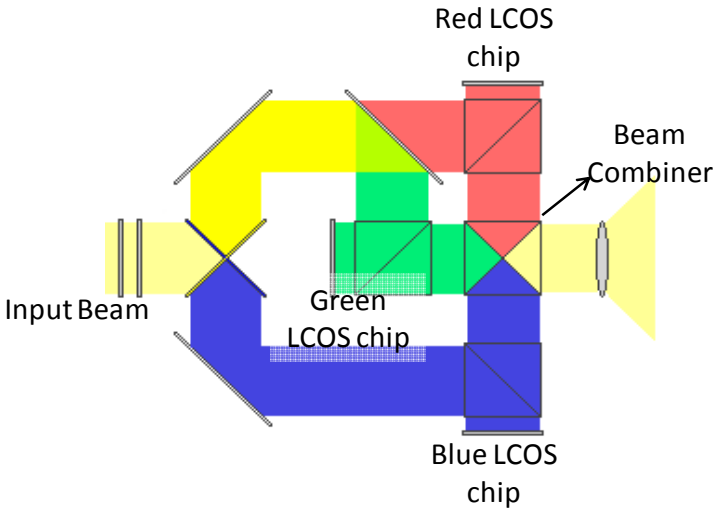

Figure 3.12 The figure shows the schematic drawing of the LCOS unit. The unit includes filters to seperate the white light into seperate colors and then to combine the beams together after each beam is reflected from the corresponding LCOS chip

The LCOS unit of a LCOS projector is reverse engineered in order to use in the Light Engine. The reasons for not using a commercial LCOS unit are:

- The alignment difficulty of the three LCOS chips
- Special filter requirement for separating and combining beams
- The difficulty of synchronizing the LCOS chips with the other Light Engine parts by using the given commercial LCOS driver

The general specifications of the LCOS unit used in the Light Engine were found from the datasheets and they are given in Table 3.10. In order to better understand the inner structure and to measure the critical distances, the LCOS unit of the projector was dismantled. The measured distances are shown in Figure 3.13.

LCOS Unit	
Resolution	SXGA+(1400x1050)
LCOS Chip Size	0.7” diagonal
Pixel Size	10.16µm x 10.16µm
Horizontal Scanning Frequency	15-100 kHz
Vertical Scanning Frequency	50-100 Hz
Dot Clock	170 MHz

Table 3.10 Specifications of the LCOS unit

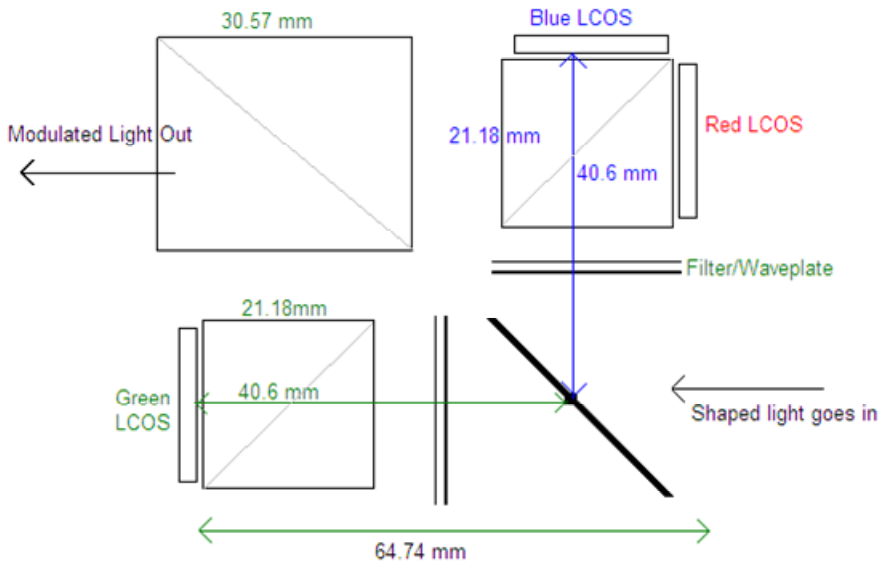

Figure 3.13 Optical layout of the LCOS unit including critical distances

The filter oriented at 45° transmits green and reflects pink. The reflected beam is divided into red and blue colors with the next filters. The maximum divergence angle of the light after it gets modulated by the LCOS unit was found to be 65mrad (3.7deg). Experiments were performed to study the state of polarization of the light after it enters the LCOS unit. Based on experiments, the green light going into the system was found to be vertically polarized while the red and the blue lights were horizontally polarized. When the laser beams without these polarization states are sent to the system, most of the beams cannot reach the output. Therefore the polarization of the used lasers should be adjusted (rotated if necessary) before sending their output into the LCOS unit.

3.6 Projection Lens

The projection lens focuses the scanned image columns reflected off the LCOS devices on to the Intermediate Image stage. The lens is required to create a 20” projection at

500mm; therefore a magnification of around 25X is needed. The projection lens of the dismantled projector was checked for these specifications. Its performance was within the required limits therefore it was chosen as L1 for the Light Engine. The specifications of the projection lens are given in Table 3.11 and the measured distances are shown in Figure 3.14.

Projection Lens	
Focal Length	21.7-35.8mm
F-number	1.85-2.5
Lens Shift	9:1, Fixed
Zoom	1.7X Powered
Projection Distance Coverage	1.2-9m
Number of elements	12
Number of lens groups	6
Number of moving groups	4

Table 3.11 Specifications of the projection lens

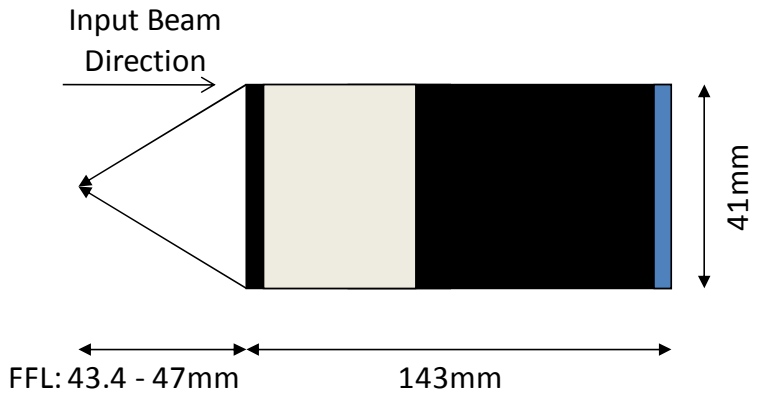

Figure 3.14 Dimensions and the measured front focal length of the projection lens

3.7 System Efficiency

After the components for the first and the second prototype were selected, a spread sheet was prepared to calculate the expected system efficiency. The major assumptions that were made during the evaluation of the system efficiency are:

- The efficiency of the optical components assumed to be independent of the wavelength.
- The efficiency values are not taken from data sheets. Typical values are used in the data sheet. (e.g. 95% for regular lenses, 95% for regular beam splitters)

This study was done in order to calculate the maximum efficiency and the maximum perceived output brightness that the system can have. Also the required power levels of RGB lasers were checked. The calculated and the measured efficiency of the Light Engine are given in Figure 3.15. The capital letters next to specific components show the polarization direction changes. The green laser's polarization does not change through the optical train; therefore the efficiency for the green path is higher than the red and the blue path.

	Component	% Efficiencies RED		GREEN		BLUE	
	Wavelength	**640 nm**	**V**	**532 nm**	**V**	**465 nm**	**V**
Part 1 Laser Beam Shaping and Combining Unit	Laser lenslet array	90%		90%		90%	
	Field lens 1	95%		95%		95%	
	X-cube	80%		80%		80%	
	Field lens 2	95%		95%		95%	
	Uniformizer lenslet array1	90%		90%		90%	
	Uniformizer lenslet array2	90%		90%		90%	
	Field lens3	95%		95%		95%	
	Scanner	90%		90%		90%	
	Field lens4	95%		95%		95%	
	Efficiency of Part 1	**43%**		**43%**		**43%**	
Part 2 LCOS Unit and Projection Lens	Colour separating mirror	80%		80%		80%	
	Polarization rotator	80%	H/V	100%	V	80%	V/H
	Polarizing Beam Splitter	95%		95%		95%	
	LCOS Panel	65%	V/H	65%	H	65%	H/V
	Polarizing Beam Splitter	95%		95%		95%	
	Polarization rotator	80%	V	100%	H	80%	V
	Colour Combining PBS	90%		90%		90%	
	Projection Lens	85%		85%		85%	
	Efficiency of Part 2	23%		36%		23%	
	Efficiency of Part 2 Measured	**27%**		**29%**		**14%**	
	Total Efficiency (Expected)	**10%**	V	**15%**	H	**10%**	V
	Total Efficiency (Measured)	**11%**		**12%**		**6%**	

Figure 3.15 The measured and the calculated efficiency of the Ligth Engine. The capital letters next to the components show the changes in the polarization direction (V:vertical, H: horizontal)

4 OPTICAL DESIGN OF THE LIGHT ENGINE

The optical design of the Light Engine was done by the optical simulation program ZEMAX™. The results of the simulations and the assumptions taken during the modeling of critical parts are given in this section.

4.1 Design of a Scanning System

The first design effort in ZEMAX™ was modeling a scanning system in which a laser line is scanned onto the image plane as shown in Figure 4.1.

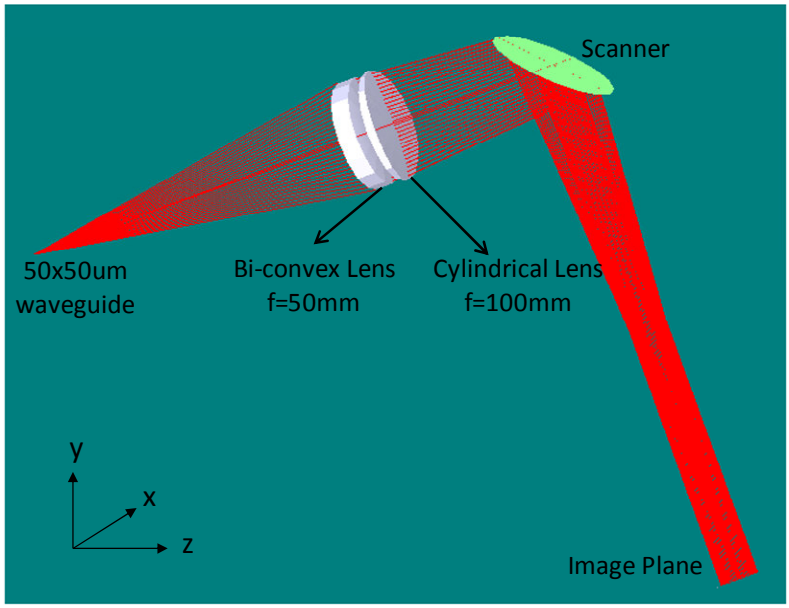

Figure 4.1 Shaded model of a laser scanning based system

This system is designed in the “Sequential Mode” of ZEMAX™. For the simplicity, the design was done for a single color and the source assumed to be a light guide with

dimensions of 50x50 um. As it is shown in Figure 4.2, the light guide is modeled by using five different field points located at the edges and the center of a square. The beams coming from the waveguide are collimated by a bi-convex lens and a laser line is created by a cylindrical lens. The scanner makes a ±2.5° mechanical scan angle and scans the created laser line onto the image plane. "Tilt and De-center Elements" tool is used to crate 45° tilted mirror and "Multi Configuration" editor is used to move the scanner to 2.5°, 1.25°, 0°, -1.25°, -2.5° scan angles.

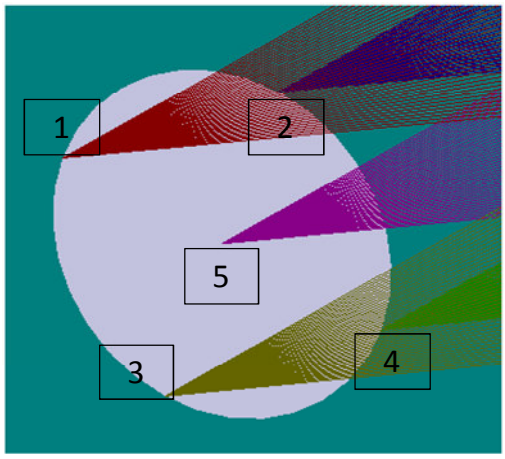

Figure 4.2 Modelling of a waveguide source with five different field points

The semi-diameter and the focal length of the biconvex lens were chosen such the length of the created line is between 10 – 15 mm. The spot diagram of the resulted lines for the five scan angles is shown in Figure 4.3. As it can be seen from the zoomed version of the laser line for the 0° scan angle, the laser line is thick at the center (400µm) and gets thinner at its edges. The reason for this behavior is the geometrical aberrations caused by using single lenses with non-optimized surface profiles.

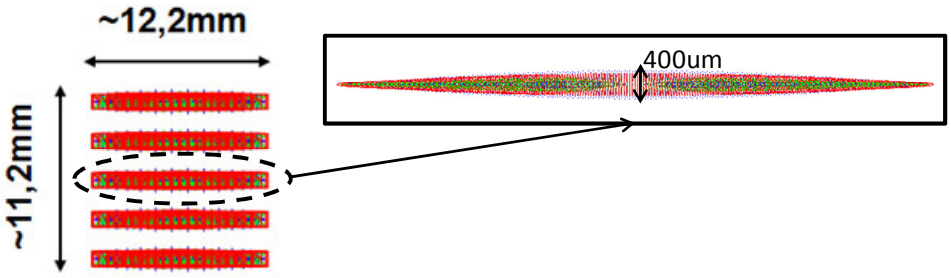

Figure 4.3 The spot diagram of the laser lines created at the image plane. The five different lines correspond to different scan angles.

This design study shows the method of creating and analyzing a laser scanning based system in ZEMAX™ and the importance of using optimized and well-designed lenses in order to create a thin laser line without aberrations.

The performance of a lens can be understood by looking at the FFT-MTF analysis. This analysis gives information about the spatial frequency supported by the optical components. The Light Engine projects a 20" diagonal image with a 1400x1050 resolution. Along the length of the display there are 700 cycles (one pixel on and one pixel off) over 406.4mm. According to these values, the lenses used in the display should support a spatial frequency of 1.72 cycles per millimeter. The FFT-MTF analysis of the collimating lens explained above is given in Figure 4.4. As it can be seen from the figure, the collimating lens used in the analysis does not support the required spatial frequency.

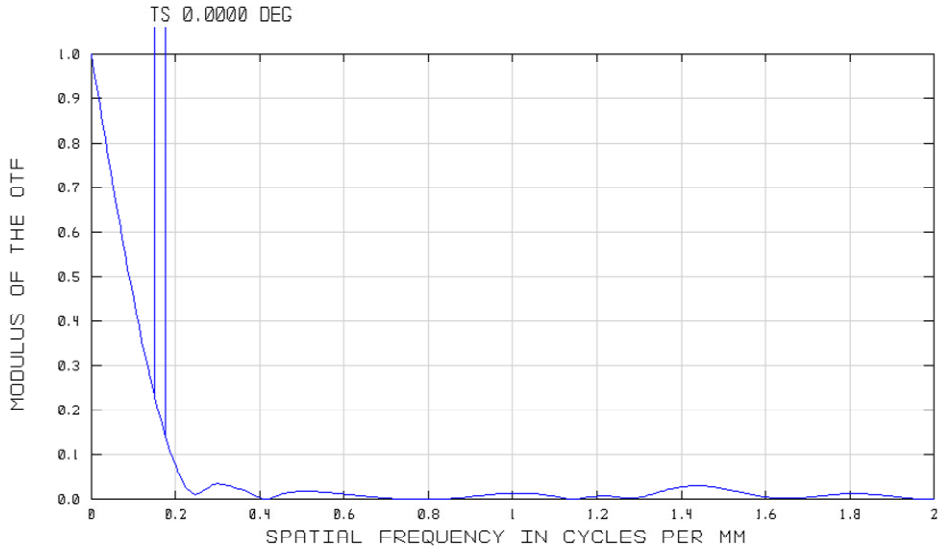

Figure 4.4 FFT-MTF Analysis of the collimating lens. The lens can support spatial frequencies up to 0.2 cyc/mm

4.2 Design of the Projection Lens

The projection lens used in the Light Engine is taken from a commercial projector and most of its specifications are unknown. The projection lens consists of twelve lenses with four moving parts. The lenses are in a metal housing which cannot be opened without damaging the lenses. In order to model the projection lens, different lens recipes from lens design books were tried and then optimized to have similar specifications (magnification, lens diameter, imaging quality, etc.) with the projection lens in collaboration with Dr. Kishore V.C. The ZEMAX model of the projection lens is given in Figure 4.5. The design works similar to the original projection lens but its diameter is smaller than the actual lens and it can support a magnification of 14.7X. The performance of the designed lens is less than the actual projection lens but this is an expected result since the designed unit has less lenses compared to the original unit and does not have any moving parts.

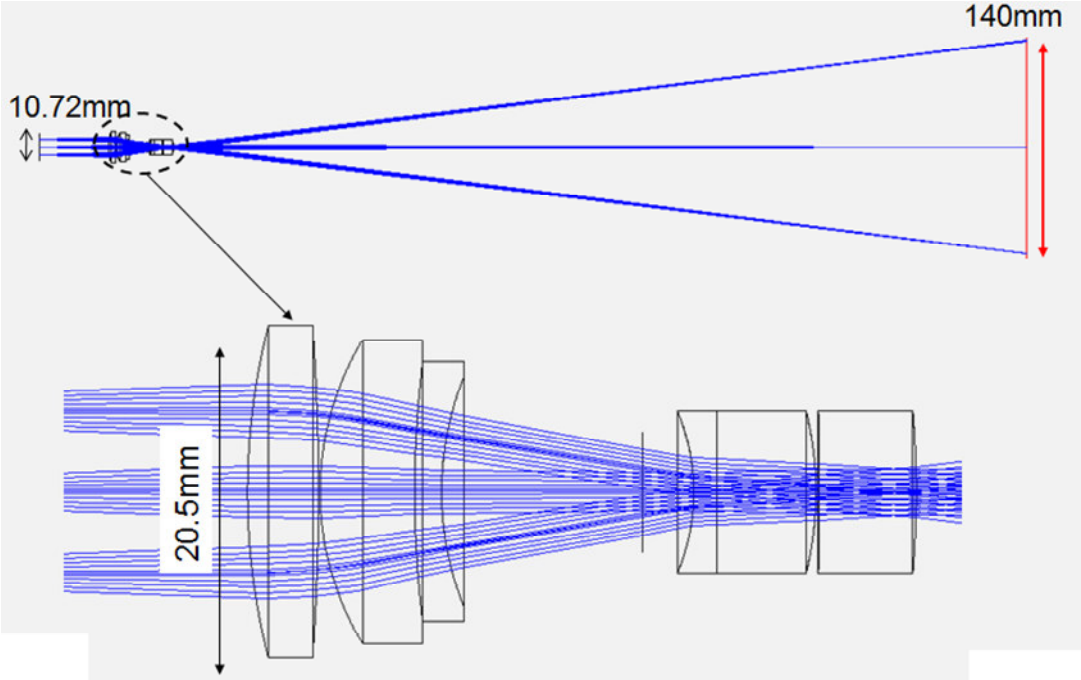

Figure 4.5 The ZEMAX™ model of the designed projection lens

The performance of the design was analyzed by using FFT-MTF, Spot Diagram and Geometric Image Analysis tools. The results of the analysis are shown in the figures below.

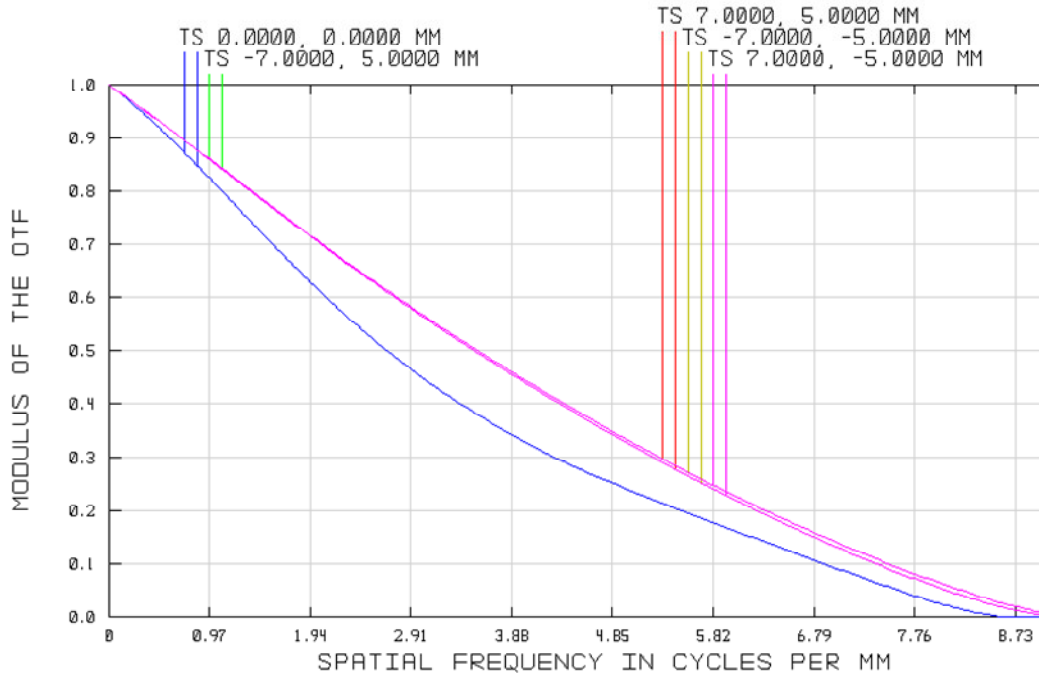

Figure 4.6 The FFT-MTF analysis of the projection lens

As it can be seen from Figure 4.6, the projection lens can support spatial frequencies up to seven cycles per millimeter. The calculated spatial frequency was 1.72cyc/mm, therefore this design is valid even if the resolution of the system is increased or the projected image size is decreased.

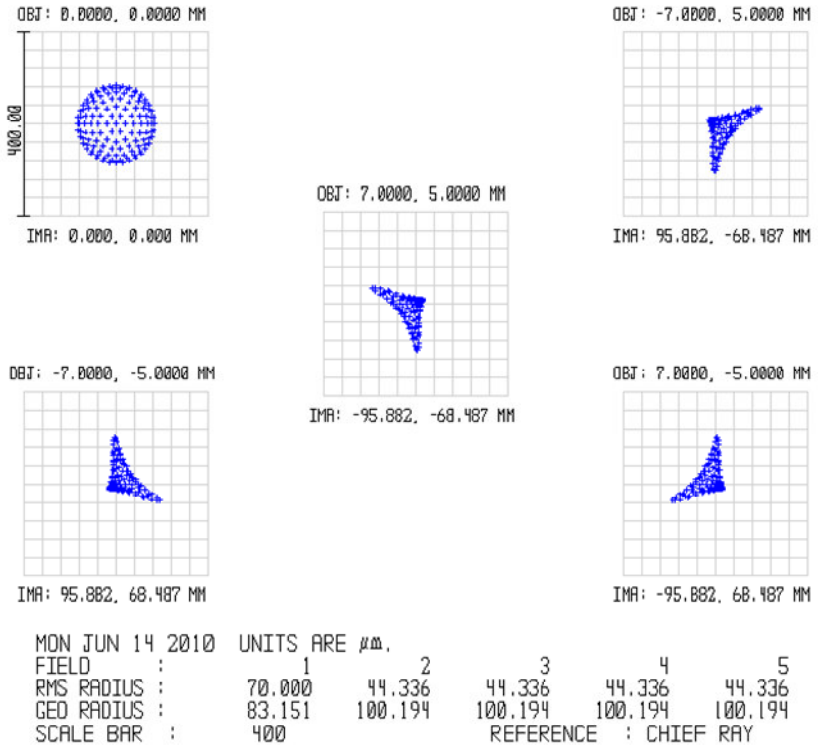

Figure 4.7 Spot diagram of the projection lens. The different field points correspond to the locations of the corners and the center of the LCOS chip.

The spot diagram given in Figure 4.7 shows the shape and the size of the spots formed by the beams coming from five different field points. The field points correspond to the locations of the corners and the center of the LCOS chip. The spots of the corners show some aberrations but the size and the shape of the spots do not show major changes even though the beams leave the lens with 14° (full angle). In order to measure the imaging performance of the projection lens, geometric image analysis was performed.

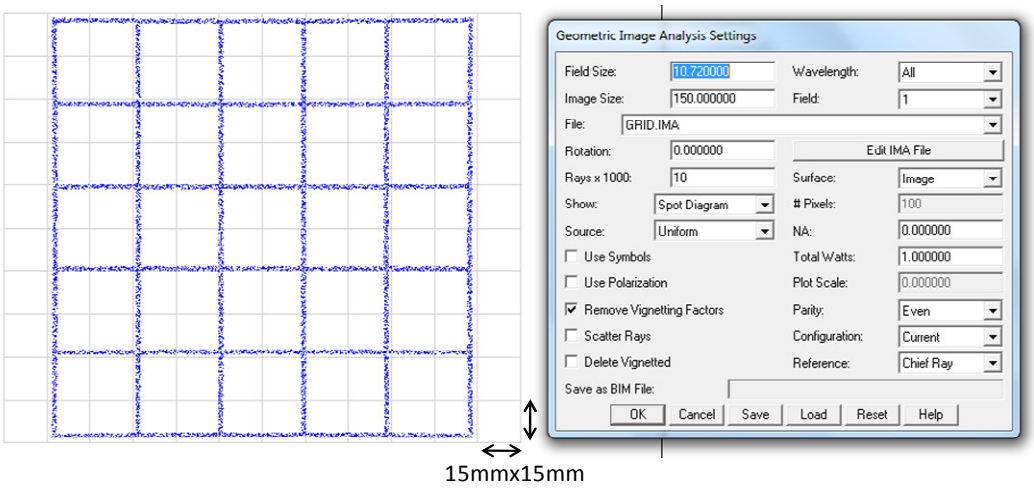

Figure 4.8 Geometric image analysis of the projection lens (left) and the settings used in the analysis (right)

In the geometric image analysis, an image (for this case a square with grids) is sent to the system and the output at the image plane is showed. As it can be seen in Figure 4.8, the image does not show disturbing aberrations or distortions. After checking the performance of the projection lens design by using the analysis methods given above, the specifications of the projection lens were used in the whole system design.

4.3 Design of the X-cube

The modeling of an X-cube in ZEMAX™ can be done by creating polygon objects. Polygon objects are created by defining the vertices of a collection of triangles in 3D space. In order to construct a polygon object, individual faces or face groups of the object are defined. An X-cube can be created by defining eight vertices and then connecting each of these vertices using the rectangle symbol supported by the polygon object in ZEMAX™. The designed model of the X-cube is shown in Figure 4.9.

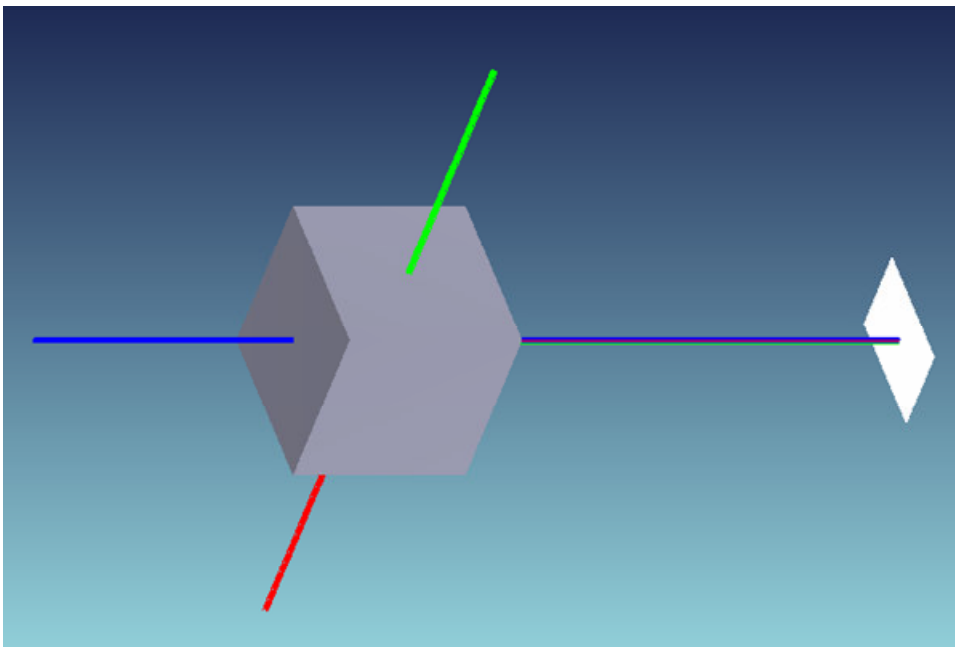

Figure 4.9 The shaded model of the X-cube designed by using polygon objects
The size of the designed X-cube is 4x4x4cm

4.4 Design of the LCOS unit

The LCOS unit was modeled by manipulating the input beams by using dichroic coatings, polarizers and wave plates. The design of the LCOS unit with a scanning beam input is shown in Figure 4.10.

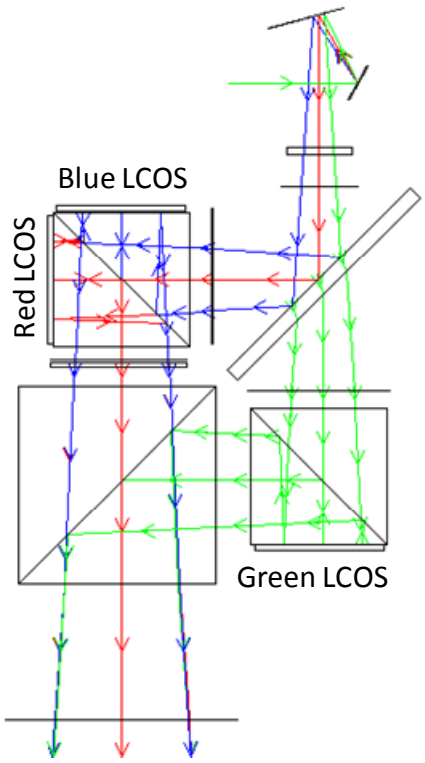

Figure 4.10 The design of the LCOS unit. The beams are combined together after getting reflected from the LCOS chips

4.5 Design of the Beam Homogenizer

The design of the beam homogenizer includes choosing appropriate specifications for the fly's eye homogenizer illustrated in Figure 3.8. The pitch of the laser lenslet array has to match the spacing between the emitters in a laser column. A mismatch causes beams to spread around and most of the brightness is lost. The second critical parameter in the design is the distance between FL1-FL2 and FL3-FL4. The distances have to be equal to one focal length for each group. The focal length of FL3 and FL4 determines the size of the output beam. The pitch of the uniformizer lenslet arrays is not very critical but in

theory the amount of homogenization increases as the pitch decreases. The design of the beam homogenizer for green Necsel™ laser is given in Figure 4.11. The intensity difference between the two laser lines is due to the difference between the beam waist locations of the two laser columns. If the distances are adjusted correctly, the output of the homogenizer propagates almost collimated.

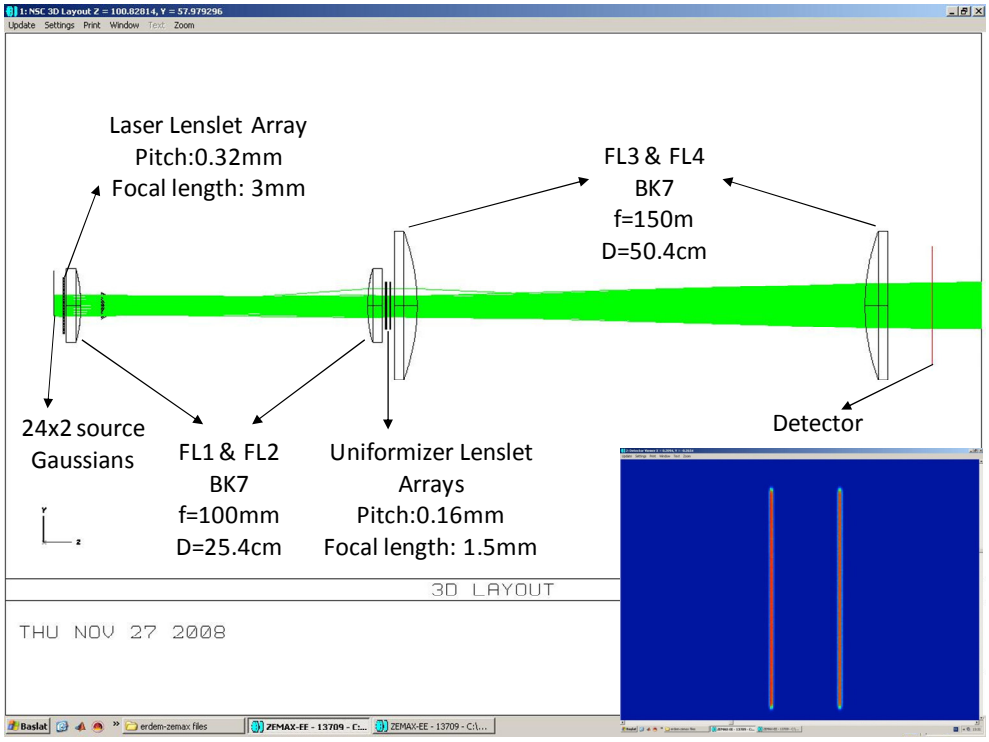

Figure 4.11 Design of the fly's eye beam homogenizer and the detector view

This design study shows that it is possible to obtain a homogenized laser line from a multi emitter laser by using a fly's eye beam homogenizer. The profile of one of the created laser lines is shown in Figure 4.12. As it can be seen from the figure, the beam has a uniform profile along the laser line axis but keeps its Gaussian shape on the other axis.

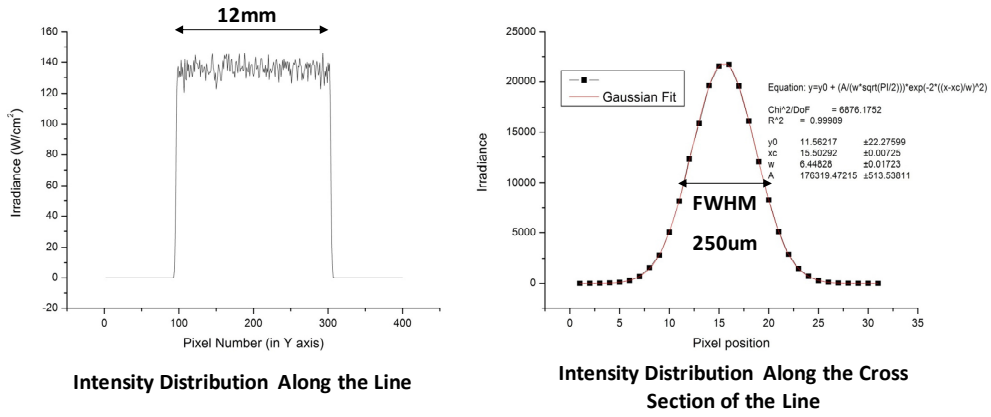

Figure 4.12 The calculated intensity distribution at the detector plane of the fly's eye beam homogenizer.

4.6 Design of the First Prototype

A preliminary laser line generator is designed for a single laser before modeling a full system with prototype 1 lasers. The design was done for the green which has a beam diameter of 2mm and a full divergence of 1.5mrad. An expander is used to expand the beam and decrease the divergence angel even further. After the expansion, the laser line is created by a cylindrical lens. The intensity profile of the laser line at the image plane is given in Figure 4.13.

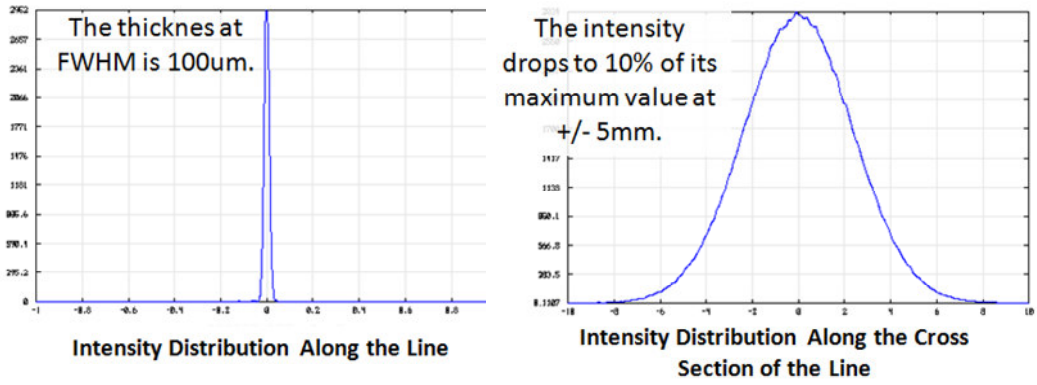

Figure 4.13 The calculated intensity distribution for a single color at the first prototype

The intensity profile along the line is not uniform in the first prototype. The profile of the beam stays Gaussian due to the lack of a beam homogenizer. In order to reduce the intensity variation, the size of the line can be increased and the edges can be cut. If the Gaussian beam has a spot radius of w and it passes through an aperture with radius a, the power transmission can be calculated as:

$$\text{Power Transmission} = 1 - e^{-2a^2/w^2} \tag{4-1}$$

After analyzing the laser line properties for a single color, the design of the whole system for the first prototype was finished. The optical design of the first prototype can be seen in Figure 4.14.

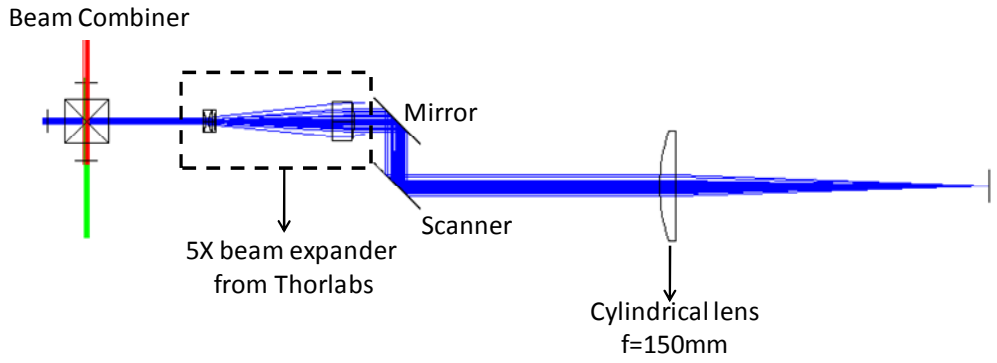

Figure 4.14 The optical design of the complete first prototype

4.7 Design of the Second Prototype

After designing the separate key components, the design of the complete second prototype was finished by collaborating Dr. Kishore V.C. and it is given in Figure 4.15.

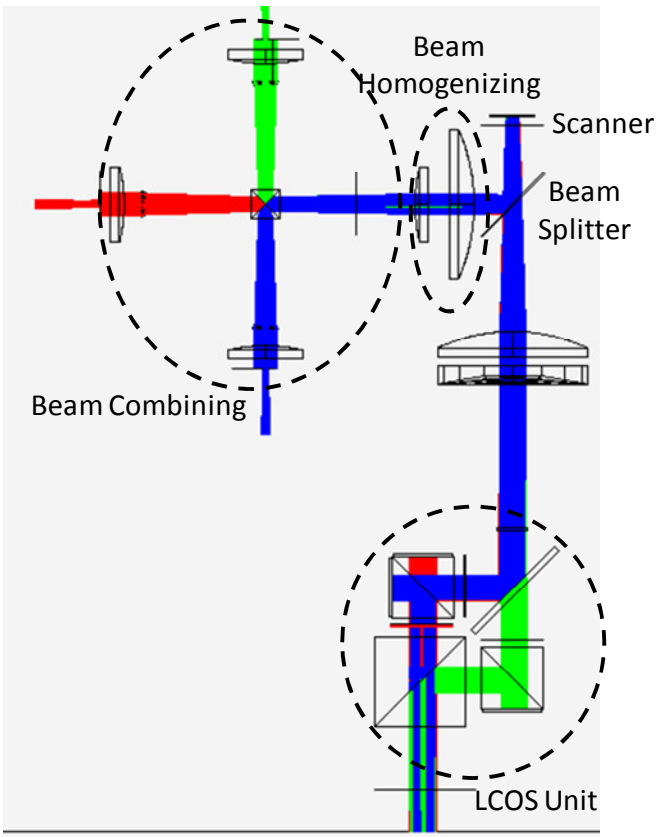

Figure 4.15 Optical design of the second prototype

The figure includes some assumptions in order to make the schematic clearer. The actual system does not a beam splitter and the laser line hits a scanner which is located 45° tilted with respect to laser propagation plane; therefore the LCOS plane is actually located at some plane into the page. In order to draw everything at the same plane, the configuration of the scanner was changed. The design of the Light Engine including the projection lens is given in Figure 4.16. The design in the figure includes an f-theta lens to control the incident angle at the LCOS plane. In the actual set up, the LCOS unit can

handle the incidence angle coming from the scanner (±2° mechanical); therefore no f-theta lens is used.

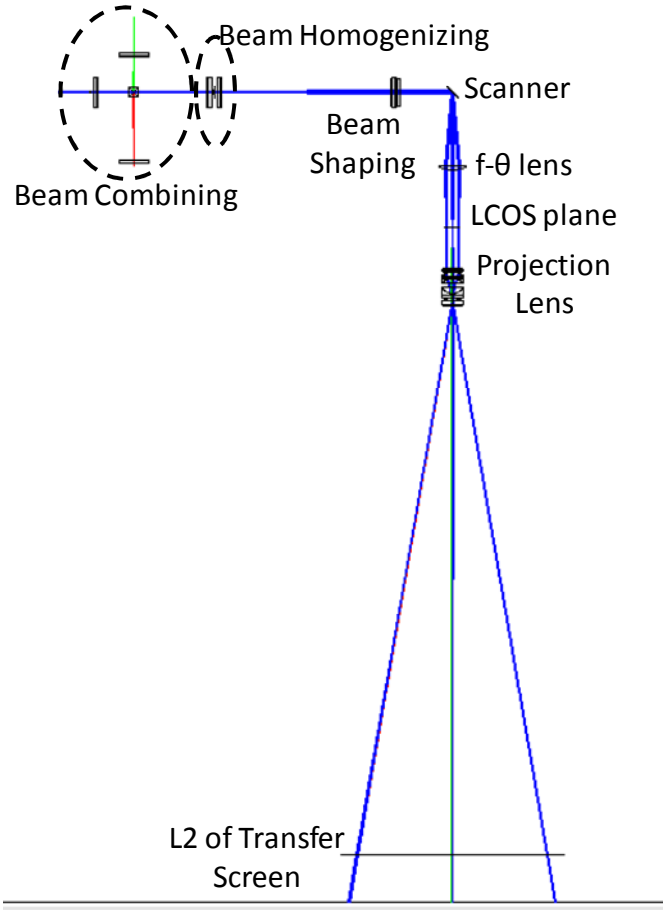

Figure 4.16 Optical design of the second prototype including the projection lens

4.8 Design of a Fiber Coupler for a Multi Emitter Laser

Although a free space approach is adapted for the Light Engine, a fiber coupler for the Necsel™ lasers was also designed by Dr. Kishore V.C. The specifications of the designed coupler are given in Figure 4.17. The divergence of the output beams are controlled by the

lens array and three lenses are used to focus the beams into the fiber. The first two lenses are used to decrease the numerical aperture so that the final lens can focus the beam to a smaller area.

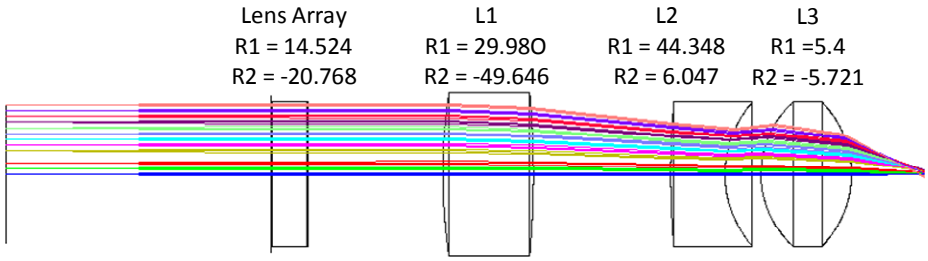

Figure 4.17 Fiber coupler design for Arasor lasers

After designing the fiber coupler, the physical optics propagation is used to compute the fiber coupling efficiency. The menu for evaluating the coupler is available from Zemax > Analysis > Physics Optics > Physical Optics Propagation. This menu allows the definition of the input beam, the fiber and the beam positioning.

The Merit Function operand POPD reports the coupling efficiency. The beam used was a multimode beam made up of 24 beamlets with 0.04mm waist. One of the key parts is the x-width and y-width, which should be entered manually for a custom beam (they are set automatically for a single beam). X-width and y-width defines the guard band, which is an empty space around the beam where the beam can freely expand as it propagates. The efficiency of beam coupling depends on the x and y widths. In order to get more reliable results, a single Gaussian beam was used to propagate inside the system and ZEMAX automatically defined the initial size. Then the efficiency for different field points was read from the values column in the Merit Function Editor window.

5 EXPERIMENTAL RESULTS

The main experimental work at the beginning of the project was dismantling an LCOS projector and replacing its light source with lasers. After preparing the projector, experiments were done to measure the critical distances of the projector (e.g. the distance from the LCOS unit entrance to the LCOS chips) and to determine the specifications of the components in the optical train (type, transmission ratio, working polarization direction etc.). The other task related to the projector was characterizing the projection lens. The results of these experiments were used to model the system in ZEMAX™ and to calculate the system efficiency. The information regarding these steps can be found in the previous sections.

5.1 Single Color Demonstration

After characterizing the LCOS projector, the next step was driving the LCOS unit with a scanning laser line and observing for any image artifacts. A single emitter high power (in the order of a few Watts) green laser is used to create a laser line. Most of the components were not available at the date of the experiment; therefore the laser line is created by using two cylindrical lenses placed 90° rotated with respect to each other. The first cylindrical lens was determining the length of the line while the second cylindrical lens was focusing the beam on the other axis to create a thin laser line. The laser line was scanned with a FR4 scanner [85, 86] driven by a sinusoidal input. The setup used for a single color demonstration is shown in Figure 5.1.

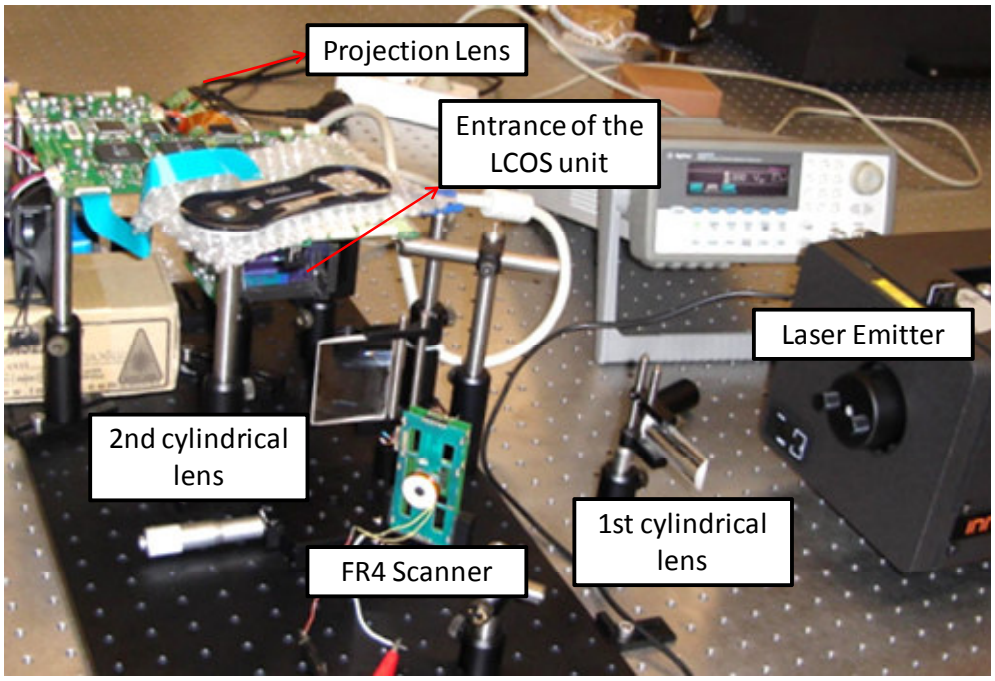

Figure 5.1 Light Engine single color demonstration setup

The experiment was conducted by using a green laser; therefore special image content is prepared and sent to the projector with help of a computer. The prepared content and the image formed on the screen can be seen in Figure 5.2. Some of the beams reflected from the lenses and fell on the screen (bright areas at the upper left and lower left of the image). The optical power output of the laser was 300mW during the data capture. The power was increased up to 1W to check the damage threshold of the LCOS unit.

Then a video content was sent to the projector to check for flickering or frequency mismatch. The scanner's frequency was swept from 0.5Hz to 70Hz and starting from 30Hz, no flicker effects were observed.

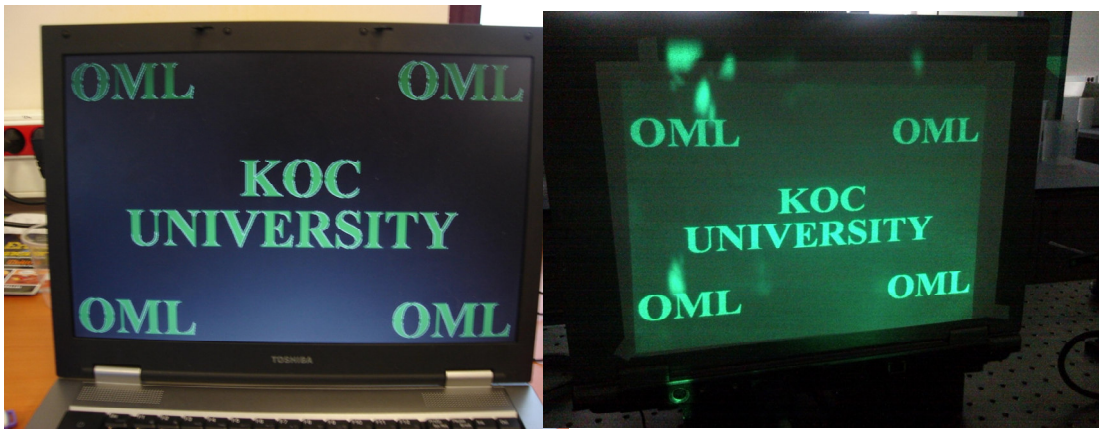

Content send by the computer Image on the White Screen

Figure 5.2 Light Engine single color demonstration results

This demonstration shows the compatibility of the LCOS unit to the laser scanning illumination. It also shows the amount of degradation in the image quality caused by the speckle. Speckle is a common problem in laser based displays and a discussion of the speckle formation and the speckle reduction methods can be found in Appendix A.

5.2 Three Color Demonstration

Red, green and blue lasers with single emitters were used to build the first full color prototype of the Light Engine. The uniformity of the scan line was checked by ZEMAX™ design prior to building the system and the system was built based on the optimized distances with the help of Selim Ölçer. A red laser beam with a 3 mm beam diameter and 0.8mrad half divergence angle is combined with green and blue lasers with 2 mm beam diameters and 0.75mrad half divergence angles using an X-cube as shown in Figure 5.3. The polarization direction of the green and the red lasers was not in the correct state. This could cause a poor light coupling to the LCOS engine; therefore two half-wave plates were used to correct the plane of polarization of the lasers.

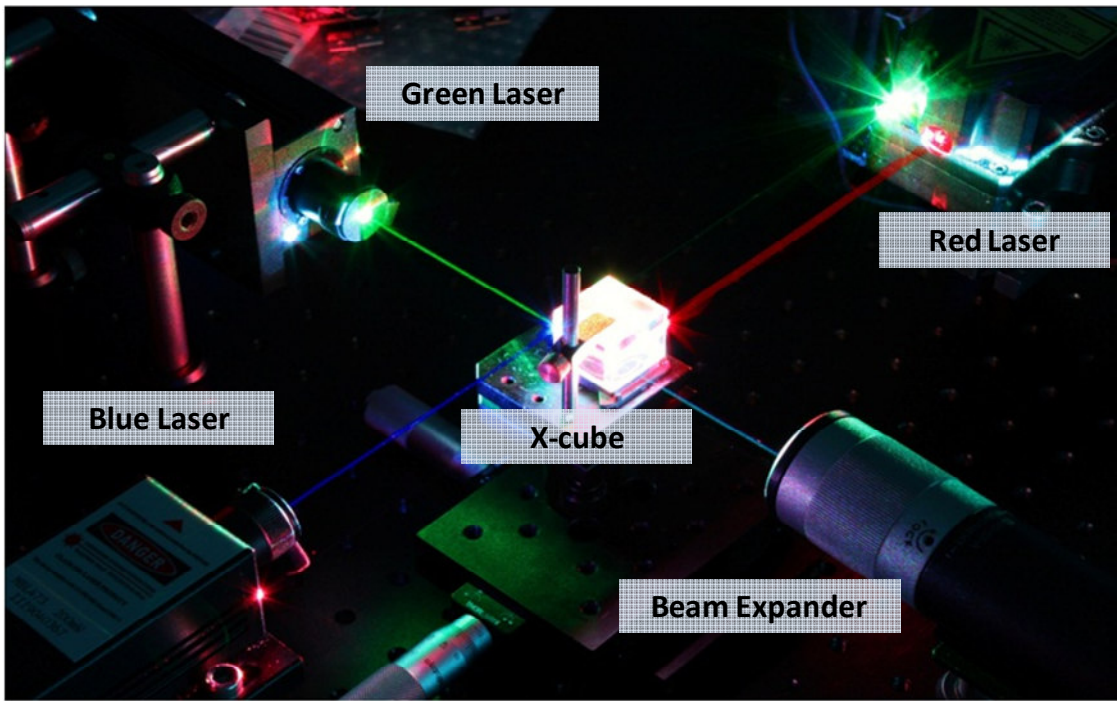

Figure 5.3 RGB Laser beam combining with an X-cube

The combined beam is then expanded with a 5X beam expander and scanned with a 1D scanner over the LCOS unit with ±1.36° mechanical scan angle. Figure 5.4 shows the output of the beam expander, the cylindrical lens with 150 mm focal length, the scanner and the entrance of the LCOS unit.

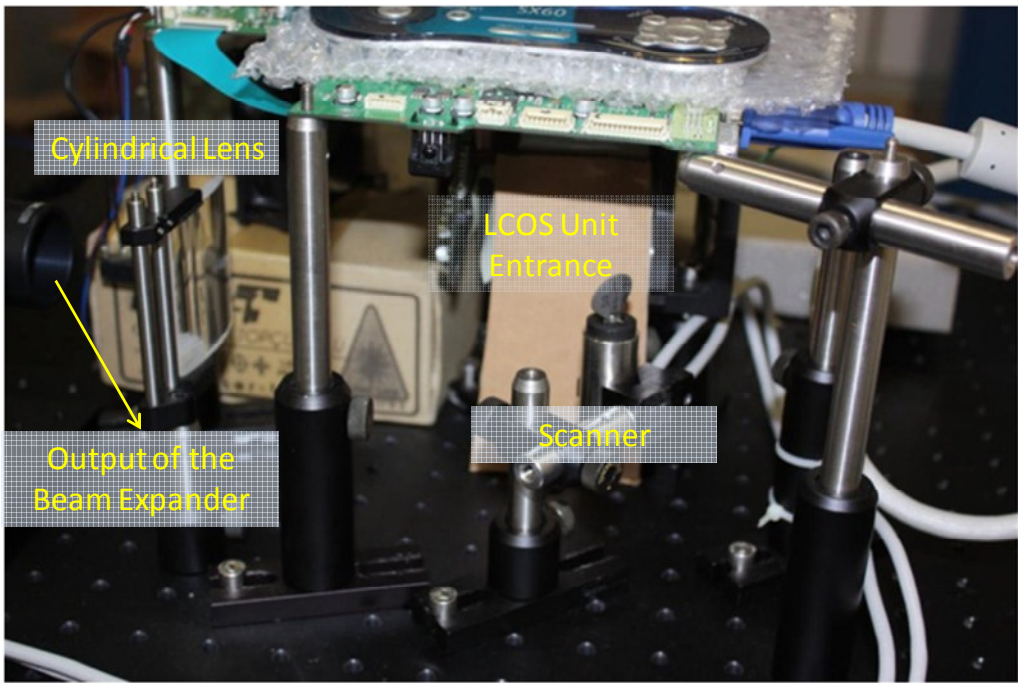

Figure 5.4 Laser line creation and scanning part of the first prototype

The beam width of the red laser is different from the green and the blue lasers. When the laser beams are combined, the red laser line does not perfectly overlap with the other two lines. However, since the laser line is scanned across the horizontal direction, time averaging reduces any display artifacts due to color mismatch in the horizontal direction. The difference in the beam size along the vertical direction changes the intensity of the beam on LCOS plane and increases the difficulty of the white balancing. Approaches such as using a Gaussian to top-hat convertor or using individual beam expanders for each laser were also considered to improve image quality for the first prototype. The problem with a Gaussian to top-hat convertor is that it has a certain working distance and the beam diverges after that point. An increase in beam divergence increases the width of the line at

the LCOS panel and can cause crosstalk; therefore this approach was not pursued. Using separate beam expanders for each laser can produce a better color balance across the screen by increasing the precision in the alignment but this increases the cost and the complexity of the system. The second prototype will utilize multiple emitters and micro-lens array based homogenizers so it was decided not to invest further effort in the beam homogenization for Prototype 1 as the components will not be reusable for Prototype 2.

As it can be seen in Figure 5.5, even though the system had no beam homogenizer, the intensity along the image width does not change abruptly. The image on the white screen has a size of 20" diagonal. The circular area on the screen is due to damage on one of the coatings in the LCOS unit. This coating was on the path of blue and red channels; therefore the circular region was dominated by the green color and the white balance of the final image got distorted. Also there are some image artifacts caused by the speckle but the speckle contrast is expected to be reduced by a factor of $\sqrt{N}$ with the use of new multi emitter lasers where N is the number of the emitters. The theoretical reasons behind this reduction can be found in Appendix A.

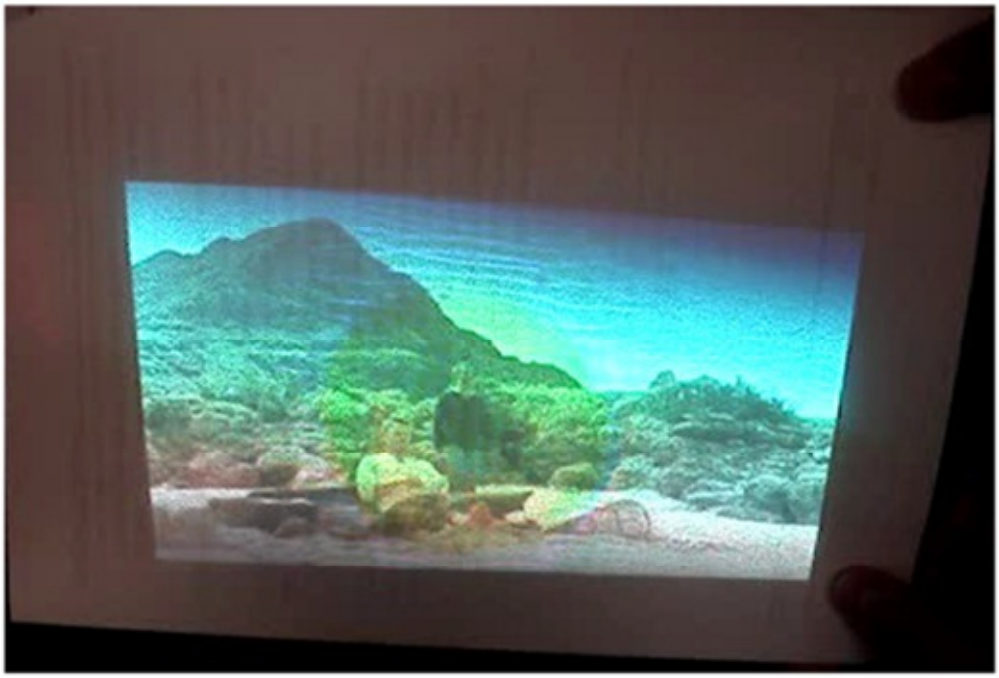

Figure 5.5 Image projected with the Light Engine on a diffuser screen. The image produced is 20” diagonal. Green haze and lines in the middle of the screen are verified to be due to a damage on the coating

6 CONCLUSIONS & FUTURE WORK

This thesis reports the results of design, development, characterization and modeling of a new laser projection unit for a novel autostereoscopic 3D display. The main differences of the proposed 3D display from the conventional commercially available 3D displays are no special glass requirement, the “look around” capability gained with the use of a high accuracy and low latency pupil tracker, the 2D compatibility when it is desired or the number of viewers is more than the limit and the use of lasers as the light source.

Different types of lasers that can be used in displays have been analyzed. After checking the requirements for the display, two groups of lasers for the first and the second prototype have been acquired. The power ratios for the chosen laser wavelengths and the total output luminance have been calculated. The required optical power for each primary color to create a white color at 6500K has been reported.

Three different laser beam combining methods have been discussed. A free space approach has been found most suitable for the Light Engine. The characterization of an X-cube has been done experimentally and was used in the first prototype of the display.

The design of the beam shaping and the homogenizing parts of the display for the single emitter lasers of the first prototype and the multi emitter lasers of the second prototype have been completed. Regular optical elements such as a beam expander and cylindrical lenses are used to create a line for the first prototype. A fly’s eye beam homogenizer is adapted to create a uniform laser line from multi emitter lasers of the second prototype.

An LCOS projector has been dismantled and the critical distances, the transmission ratios of the components inside and the polarization directions have been measured

experimentally. The lamp of the projector was removed and a commercial galvanometric scanner is used to scan a laser line into the LCOS unit.

The ZEMAX™ design of the Light Engine for the first and the second prototype including all the components has been completed. The design was used to determine the performance of the system, measure the theoretical profile of the created laser line and to calculate the power density for checking the damage threshold of certain components.

The optical hardware of the first prototype has been completed and the results have been demonstrated. The damage on one of the coatings created a circular shade and some cracks on the image and created some regions with color mismatch. Also, speckle and the lack of a beam homogenizer decreased the quality of the image but no critical problems related to system's working principle or chosen components have been observed. Prototype 1 showed that a LCOS based display engine can be driven by a laser line and scanned by a scanner that is working at 60Hz without causing any disturbing display artifacts. The system was delivered to UCL for integration with the transfer screen module and the head-tracker for full 3D display functionality demonstrations.

In order to build the second prototype, the components including the lasers and the micro-lens arrays have been acquired. The procurement (design and fabrication when necessary) of the opto-mechanic components for holding and aligning these components has also been finished.

The next step of the project is building a Light Engine with the high power multi emitter lasers. Implementing a beam homogenizer, changing the damaged LCOS unit with a new one and using multi emitter lasers are expected to solve the image quality problems observed in the first prototype.

APPENDIX A: SPECKLE & SPECKLE REDUCTION TECHNIQUES

A.1 Speckle Formation in Laser Displays

When an object is illuminated with a coherent light source, such as a laser, the scattered light has components with different delays which are caused by the roughness of the illuminated surface. As the scattered light propagates further, these coherent but de-phased components interfere and produce a granular intensity pattern called speckle on the screen [87]. Speckle formation in free-space and in imaging systems is shown schematically in Figure A.1.

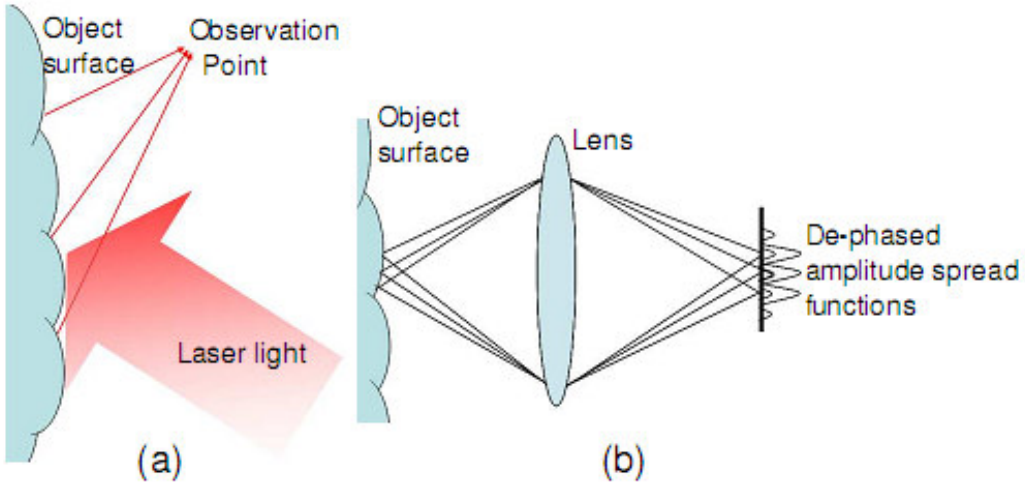

Figure A.1 Speckle formation in free space (a) and in an imaging system (b)

The shape and the linear dimensions of the speckle pattern are governed by the roughness and the curvature of the object surface [88]. The observed speckle pattern has a

dependence on the spatial location of the viewer's eyes as well as the resolution of the visual system. The speckle pattern consists of bright spots created by constructive interference, dark spots created by destructive interference and areas with intermediate brightness levels. Although speckle formation can be beneficial in precise measurement of displacements or image reconstruction [89], it is an undesired effect in laser based display systems as it destroys the information content and reduces the resolution [90]. It is estimated that human visual system can detect speckles with a contrast value down to 4% [91]. The effect of speckle on images produced by a laser projection display and the effect of a commercial speckle reduction module are shown in Figure A.2.

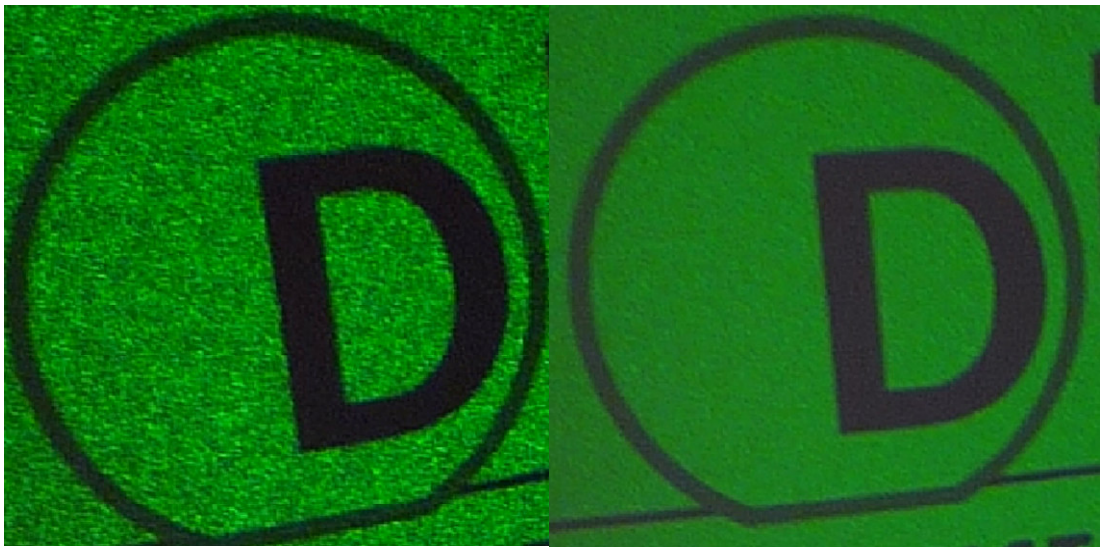

Figure A.2 Speckle on images produced by a monochrome DLP engine (left) and the effect of Dyoptyka's speckle reduction technology (Photo courtesy of Dyoptyka)

A.2 Speckle Reduction Techniques

Speckle is quantified in terms of speckle contrast which is defined as the ratio of the standard deviation of the intensity fluctuation to the mean intensity. It was shown that the addition of M uncorrelated and non-interfering speckle patterns on an irradiance basis reduces the speckle contrast by $1/\sqrt{M}$ [87]. In order to generate uncorrelated speckle patterns in the spatial dimension, incident angle, wavelength or polarization of the light source can be altered. Uncorrelated patterns in the temporal dimension can be created by placing and moving a scattering surface into the light path. The moving scattering surface creates a time varying speckle pattern and if the movement is fast enough, the speckle will be averaged out by the human eye. If the observer is close to the screen in a projection system, the perceived diameter of the speckle is typically small and speckle can be reduced by reducing the temporal or the spatial coherence of the laser. On the other hand, the average size of the speckles appears larger to the observer's eyes in the far field, therefore, small phase changes are not sufficient to eliminate the speckle [91].

Angular diversity for speckle reduction can be achieved with MEMS scanning devices working at 2-10 kHz that generates different illumination angles. Each angle of illumination provides a particular speckle image and the contrast can be reduced to half of its initial value by averaging different speckle images within the exposure time of the sensor (e.g. within 1/60 second for human eye) [92].

Using a broadband source reduces the temporal coherence and therefore, can effectively reduce speckle without causing optical loss or design complexity. However, driving multiple laser diodes individually with different wavelengths is a very complex and costly task and is not useful for a laser based television or projector system. In order to overcome this problem, a new laser diode array structure that exhibits self-induced spectrum

widening has been suggested [93]. In this method, spectrum widening is achieved by controlling the thermal crosstalk between adjacent emitters in a laser diode array. A laser projection display with a low speckle contrast of 2% can be built by using the controlled laser diode array and a diffusion film. The diffusion film is located within the screen layers and makes oscillating movement with the help of a stepper motor. Moving screen configurations for the front and the back projection displays are shown in Figure A.3.

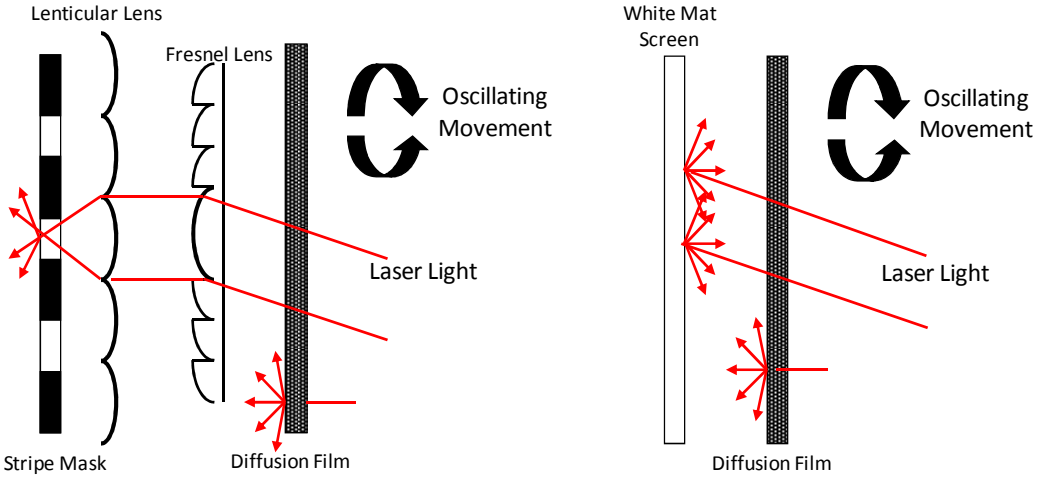

Figure A.3 Moving screen configuration for rear projection (left) and front projection (right) displays [93]

Instead of moving a diffuser or the screen, a time varying speckle pattern can be created using colloidal dispersion filled projection screens [94]. When the laser beam enters the screen, it scatters from the scattering globules inside the colloidal dispersion. A time varying speckle pattern is formed by the scattered light and this temporal averaging can lower the speckle contrast to 3%. The problem of blurring caused by the screen is reduced to acceptable levels by using highly scattering colloidal dispersion with highly forward-peaked scattering. This screen can be used with both single emitter and multi emitter lasers

and can bring additional reductions to the speckle contrast if it is combined with other methods.

Another method for creating a time varying speckle pattern is using a dynamic polymer-based diffraction grating [95]. In this approach, the diffracted light coming from the grating is collected and used as the illumination source after it is homogenized. A time-varying speckle pattern is created by the time-varying phase of the diffraction grating and subsequently averaged by a CCD camera with appropriate integration time.

The techniques discussed so far reduce the speckle contrast in considerable amounts but they do not completely remove the speckle noise and hot spot speckles remain [96]. The remaining hot spot speckles can be removed by implementing both a rotating diffuser and a running screen. This method was applied to a monochrome laser projection system a speckle contrast of 1.6% was achieved. The technique was successfully implemented in a commercial laser projection display system illustrated in Figure A.4. The image is formed by a digital light processing (DLP) system and the 70” screen is moved by a piezoelectric motor.

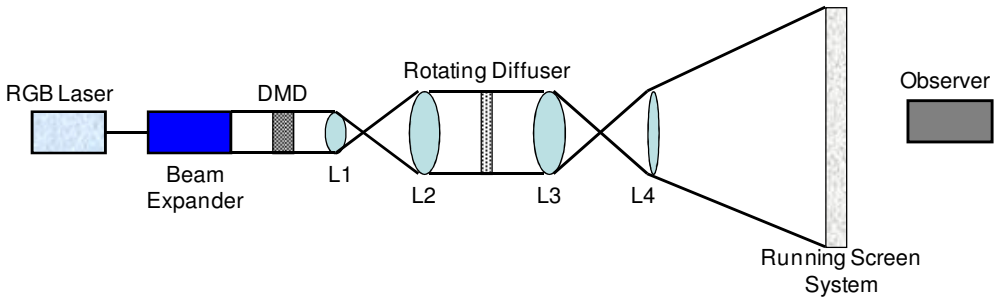

Figure A.4 Laser rear projection system with rotating diffuser and rotating screen [96]

An alternative method for reducing the speckle contrast is using non-modal, spatially incoherent beams coming from a broad-area vertical cavity surface emitting laser (VCSEL)

source [97]. The source is driven with specific current values and illuminates a polarization scrambling screen. Visible lasers, which have low spatial coherence in the far field, are required to implement this approach in laser projection applications. This method does not require the insertion of moving parts therefore the coherence of the laser and the brightness are preserved.

Instead of using general speckle reduction techniques separately, it is better to find ways of combining them together and get even lower speckle contrasts. One important parameter that needs careful attention is the type of the display system. Speckle reduction techniques with diffractive optical elements, diffusion films or screens are useful for area illuminated displays, whereas techniques using sources with reduced coherence length can be used both with area illuminated and flying spot displays.

BIBLIOGRAPHY

[1] I. Sexton and P. Surman, "Stereoscopic and autostereoscopic display systems," *IEEE Signal Processing Magazine,* vol. 16, pp. 85-99, May 1999.

[2] A. Korpel, R. Adler, P. Desmares, and W. Watson, "A Television Display Using Acoustic Deflection and Modulation of Coherent Light," *Appl. Opt.,* vol. 5, pp. 1667-1675, 1966.

[3] H. Urey, V. C. Kishore, E. Erden, and P. Surman, "State of the Art in Stereoscopic and Autostereoscopic Displays," *IEEE Proceedings,* 2010.

[4] A. J. Woods and T. Rourke, "Ghosting in anaglyphic stereoscopic images," *Stereoscopic Displays and Virtual Reality Systems XI,* vol. 5291, pp. 354-365526, 2004.

[5] I. Ideses and L. Yaroslavsky, "New methods to produce high quality color anaglyphs for 3-D visualization," *Image Analysis and Recognition, Pt 2, Proceedings,* vol. 3212, pp. 273-280, 2004.

[6] I. Ideses and L. Yaroslavsky, "Three methods that improve the visual quality of colour anaglyphs," *Journal of Optics A: Pure and Applied Optics,* vol. 7 pp. 755-762, 2005.

[7] D. W. G. Byatt, "Stereoscopic television system," United States Patent 4281341, July 28, 1981.

[8] L. Bogaert, Y. Meuret, B. Van Giel, H. Murat, H. De Smet, and H. Thienpont, "Projection display for the generation of two orthogonal polarized images using liquid crystal on silicon panels and light emitting diodes," *Applied Optics,* vol. 47, pp. 1535-1542, Apr 1 2008.

[9] L. Bogaert, Y. Meuret, B. Van Giel, H. De Smet, and H. Thienport, "Design of a compact projection display for the visualization of 3-D images using polarization sensitive eyeglasses," *Journal of the Society for Information Display,* vol. 17, pp. 603-609, Jul 2009.

[10] S. Pastoor and M. Wopking, "3-D displays: A review of current technologies," *Displays,* vol. 17, pp. 100-110, Apr 1997.

[11] E. K. Edwards, J. P. Rolland, and K. P. Keller, "Video See-Through Design for Merging of Real and Virtual Environements," in *IEEE Virtual Reality Annual International Symposium*, Seattle, 1993, pp. 223-233.

[12] V. Ferrari, G. Megali, E. Troia, A. Pietrabissa, and F. Mosca, "A 3-D Mixed-Reality System for Stereoscopic Visualization of Medical Dataset," *IEEE Transactions on Biomedical Engineering,* vol. 56, pp. 2627-2633, Nov 2009.

[13] J. P. Rolland, A. Yoshida, L. D. Davis, and J. H. Reif, "High-resolution inset head-mounted display," *Applied Optics,* vol. 37, pp. 4183-4193, Jul 1998.

[14] J. P. Rolland, M. W. Krueger, and A. Goon, "Multifocal planes head-mounted displays," *Applied Optics,* vol. 39, pp. 3209-3215, Jul 2000.

[15] E. M. Howlett, "High-Resolution Inserts in Wide-Angle Head-Mounted Stereoscopic Displays," in *Stereoscopic Displays and Applications III*. vol. 1669, J. O. Merritt and S. S. Fisher, Eds., ed, 1992, pp. 193-203.

[16] T. Sugihara and T. Miyasato, "A lightweight 3-D HMD with accommodative compensation " *SID Symposium Digest of Technical Papers,* vol. 29, pp. 927-930, May 1998.

[17] W. Robinett and J. P. Rolland, "A computational model for the stereoscopic optics of a head-mounted display," *Presence: Teleoper. Virtual Environ.,* vol. 1, pp. 45-62, 1992.

[18] F. L. Kooi and A. Toet, "Visual comfort of binocular and 3D displays," *Displays,* vol. 25, pp. 99-108, Aug 2004.

[19] O. Cakmakci and J. Rolland, "Head-Worn Displays: A Review," *Journal of Display Technology,* vol. 2, pp. 199-216, Sep 2006.

[20] I. Nyström, F. Malmberg, E. Vidholm, and E. Bengtsson, "Segmentation and Visualization of 3D Medical Images through Haptic Rendering," presented at the Proceedings of the 10th International Conference on Pattern Recognition and Information Processing (PRIP), 2009.

[21] Y. Yokokohji, R. L. Hollis, and T. Kanade, "WYSIWYF display: A visual/haptic interface to virtual environment," *Presence-Teleoperators and Virtual Environments,* vol. 8, pp. 412-434, Aug 1999.

[22] B. Grant, A. Helser, and R. M. Taylor, "Adding force display to a stereoscopic head-tracked projection display," *IEEE1998 Virtual Reality Annual International Symposium, Proceedings,* pp. 81-88 292, 1998.

[23] P. Maes, T. Darrell, B. Blumberg, and A. Pentland, "The ALIVE system: Wireless, full-body interaction with autonomous agents," *Multimedia Systems,* vol. 5, pp. 105-112, Mar 1997.

[24] W. Plesniak and M. Klug, "Tangible holography: Adding synthetic touch to 3D display," *Practical Holography XI and Holographic Materials III,* vol. 3011, pp. 53-60 370, 1997.

[25] W. J. Plesniak, R. S. Pappu, and S. A. Benton, "Haptic holography: A primitive computational plastic," *Proceedings of the IEEE,* vol. 91, pp. 1443-1456, Sep 2003.

[26] G. J. Woodgate, J. Harrold, A. M. S. Jacobs, R. R. Moseley, and D. Ezra, "Flat panel autostereoscopic displays - characterisation and enhancement," *Stereoscopic Displays and Virtual Reality Systems VII,* vol. 3957, pp. 153-164 496, 2000.

[27] R.-Y. Tsai, C.-H. Tsai, K. Lee, C.-L. Wu, L.-C. D. Lin, K.-C. Huang, W.-L. Hsu, C.-S. Wu, C.-F. Lu, J.-C. Yang, and Y.-C. Chen, "Challenge of 3D LCD displays," Orlando, FL, USA, 2009, pp. 732903-732908.

[28] M. Nishida and K. Sakamoto, "Parallax barrier 3D reflection display using polarizer slit," Boston, MA, USA, 2006, pp. 63920T-8.

[29] C. H. Chen, Y. P. Huang, S. C. Chuang, C. L. Wu, H. P. D. Shieh, W. Mphepo, C. T. Hsieh, and S. C. Hsu, "Liquid crystal panel for high efficiency barrier type autostereoscopic three-dimensional displays," *Applied Optics,* vol. 48, pp. 3446-3454, Jun 20 2009.

[30] H. Nishimura, T. Abe, H. Yamamoto, Y. Hayasaki, and N. Nishida, "Development of 140-inch autostereoscopic display by use of full-color LED panel - art. no. 64861B," *Light-Emitting Diodes: Research, Manufacturing, and Applications XI,* vol. 6486, pp. B4861-B4861 322, 2007.

[31] H. Yamamoto, M. Kouno, S. Muguruma, Y. Hayasaki, Y. Nagai, Y. Shimizu, and N. Nishida, "Enlargement of viewing area of stereoscopic full-color LED display by use of a parallax barrier," *Applied Optics,* vol. 41, pp. 6907-6919, Nov 10 2002.

[32] K. Sakamoto and T. Morii, "Multiview 3D display using parallax barrier combined with polarizer," Stockholm, Sweden, 2006, pp. 63990R-8.

[33] D. Ezra, G. J. Woodgate, B. A. Omar, N. S. Holliman, J. Harrold, and L. S. Shapiro, "New Autostereoscopic Display System," *Stereoscopic Displays and Virtual Reality Systems II,* vol. 2409, pp. 31-40 312, 1995.

[34] D. J. Montgomery, G. J. Woodgate, A. Jacobs, J. Harrold, and D. Ezra, "Analysis of the performance of a flat panel display system convertible between 2D and autostereoscopic 3D modes," *Stereoscopic Displays and Virtual Reality Systems VIII,* vol. 4297, pp. 148-159 506, 2001.

[35] D.-S. Kim, S. Shestak, K.-H. Cha, S.-M. Park, and S.-D. Hwang, "Time-sequential autostereoscopic OLED display with segmented scanning parallax barrier," Orlando, FL, USA, 2009, pp. 73290U-7.

[36] Y. H. Tao, Q. H. Wang, J. Gu, W. X. Zhao, and D. H. Li, "Autostereoscopic three-dimensional projector based on two parallax barriers," *Optics Letters,* vol. 34, pp. 3220-3222, Oct 15 2009.

[37] R. B. Johnson and G. A. Jacobsen, "Advances in lenticular lens arrays for visual display," San Diego, CA, USA, 2005, pp. 587406-11.
[38] C. H. Tsai, P. Lai, K. Lee, and C. K. Lee, "Fabrication of a large F-number lenticular plate and its use as a small-angle flat-top diffuser in autostereoscopic display screens," *Stereoscopic Displays and Virtual Reality Systems VII,* vol. 3957, pp. 322-329 496, 2000.
[39] Y. G. Lee and J. B. Ra, "Image distortion correction for lenticula misalignment in three-dimensional lenticular displays," *Optical Engineering,* vol. 45, pp. -, Jan 2006.
[40] D. K. G. de Boer, M. G. H. Hiddink, M. Sluijter, O. H. Willemsen, and S. T. de Zwart, "Switchable lenticular based 2D/3D displays," San Jose, CA, USA, 2007, pp. 64900R-8.
[41] P. Benzie, J. Watson, P. Surman, L. Rakkolainen, K. Hopf, H. Urey, V. Sainov, and C. von Kopylow, "A survey of 3DTV displays: Techniques and technologies," *IEEE Transactions on Circuits and Systems for Video Technology,* vol. 17, pp. 1647-1658, Nov 2007.
[42] T. Ando, K. Mashitani, M. Higashino, H. Kanayama, H. Murata, Y. Funazou, N. Sakamoto, H. Hazama, Y. Ebara, and K. Koyamada, "Multiview image integration system for glassless 3D display," San Jose, CA, USA, 2005, pp. 158-166.
[43] K. Mashitani, G. Hamagishi, M. Higashino, T. Ando, and S. Takemoto, "Step barrier system multi-view glass-less 3-D display," *Stereoscopic Displays and Virtual Reality Systems XI,* vol. 5291, pp. 265-272 526, 2004.
[44] H. Choi, S.-W. Min, S. Jung, J.-H. Park, and B. Lee, "Multiple-viewing-zone integral imaging using a dynamic barrier array for three-dimensional displays," *Opt. Express,* vol. 11, pp. 927-932, 2003.
[45] A. Schwartz, "Head Tracking Stereoscopic Display," *IEEE Transactions on Electron Devices,* vol. 33, pp. 1123-1127, Aug 1986.
[46] J.-Y. Son, S. A. Shestak, S.-S. Kim, and Y.-J. Choi, "Desktop autostereoscopic display with head tracking capability," San Jose, CA, USA, 2001, pp. 160-164.
[47] S. Ichinose, "Full-color stereoscopic video pickup and display technique without special glasses," *SID Proc.,* vol. 30, pp. 319-324, 1989.
[48] J. B. Eichenlaub and J. M. Hutchins, "Autostereoscopic-projection displays," San Jose, CA, USA, 1995, pp. 48-55.
[49] G. J. Woodgate, D. Ezra, J. Harrold, N. S. Holliman, G. R. Jones, and R. R. Moseley, "Observer-tracking autostereoscopic 3D display systems," San Jose, CA, USA, 1997, pp. 187-198.

[50] P. V. Harman, "Autostereoscopic teleconferencing system," San Jose, CA, USA, 2000, pp. 293-302.
[51] N. Tetsutani, K. Omura, and F. Kishino, "Study on a stereoscopic display system employing eye-position tracking for multi-viewers," San Jose, CA, USA, 1994, pp. 135-142.
[52] A. Arimoto, T. Ooshima, T. Tani, and Y. Kaneko, "Wide-viewing-area glassless stereoscopic display using multiple projectors," San Jose, CA, USA, 1998, pp. 186-192.
[53] T. Hattori, S. Sakuma, K. Katayama, S. Omori, M. Hayashi, and M. Yokoi, "Stereoscopic liquid crystal display I (general description)," San Jose, CA, USA, 1994, pp. 143-149.
[54] D. J. Sandin, T. Margolis, G. Dawe, J. Leigh, and T. A. DeFanti, "Varrier autostereographic display," San Jose, CA, USA, 2001, pp. 204-211.
[55] K. Perlin, C. Poultney, J. S. Kollin, D. T. Kristjansson, and S. Paxia, "Recent advances in the NYU autostereoscopic display," San Jose, CA, USA, 2001, pp. 196-203.
[56] Y. Takaki, "High-density directional display for generating natural three-dimensional images," *Proceedings of the IEEE,* vol. 94, pp. 654-663, Mar 2006.
[57] Y. Kajiki, "Three-dimensional display with focused light array," *Practical Holography X,* vol. 2652, pp. 106-116 360, 1996.
[58] Y. Kajiki, H. Yoshikawa, and T. Honda, "Hologram-like video images by 45-view stereoscopic display," *Stereoscopic Displays and Virtual Reality Systems IV,* vol. 3012, pp. 154-166 506, 1997.
[59] H. Urey, S. Holmstrom, and A. D. Yalcinkaya, "Electromagnetically actuated FR4 scanners," *IEEE Photonics Technology Letters,* vol. 20, pp. 30-32, Jan-Feb 2008.
[60] M. Sayinta, S. O. Isikman, and H. Urey, "Scanning LED array based volumetric display," *2008 3dtv-Conference: The True Vision - Capture, Transmission and Display of 3d Video,* pp. 1-4 388, 2008.
[61] E. Erden, V. C. Kishore, H. Urey, H. Baghsiahi, E. Willman, S. E. Day, D. R. Selviah, F. A. Fernandez, and P. Surman, "Laser Scanning Based Autostereoscopic 3D Display with Pupil Tracking," presented at the Proc. of IEEE Photonics Antalya, 2009.
[62] V. C. Kishore, E. Erden, H. Urey, H. Baghsiahi, E. Willman, S. E. Day, D. R. Selviah, F. A. Fernandez, and P. Surman, "Laser Scanning 3D Display with Dynamic Exit Pupil," presented at the Eurodisplay XXIX International Display Research Conference, Rome, 2009.

[63] P. Surman, I. Sexton, K. Hopf, R. Bates, and W. K. Lee, "Head tracked 3D displays," *Multimedia Content Representation, Classification and Security,* vol. 4105, pp. 769-776, 2006.
[64] E. Willman, H. Baghsiahi, F. A. Fernandez, D. R. Selviah, S. E. Day, K. V. Kishore, E. Erden, H. Urey, and P. Surman, "The Optics of an Autostereoscopic Multiview Display," presented at the SID International Symposium Digest of Technical Papers, Seattle, 2010.
[65] D. Gabor, "Improvements in or relating to optical systems composed of lenticules," UK Patent 541 753, 1940.
[66] V. C. Kishore, E. Erden, and H. Urey, "Laser Based Displays: A Review," *Appl. Opt.,* 2010.
[67] R. N. Hall, G. E. Fenner, J. D. Kingsley, T. J. Soltys, and R. O. Carlson, "Coherent Light Emission From GaAs Junctions," *Physical Review Letters,* vol. 9, p. 366, 1962.
[68] M. I. Nathan, W. P. Dumke, G. Burns, F. H. Dill, and G. Lasher, "Stimulated Emission of Radiation from GaAs p-n Junctions," *Applied Physics Letters,* vol. 1, pp. 62-64, 1962.
[69] T. M. Quist, R. H. Rediker, R. J. Keyes, W. E. Krag, B. Lax, A. L. McWhorter, and H. J. Zeigler, "Semiconductor Maser of GaAs," *Applied Physics Letters,* vol. 1, pp. 91-92, 1962.
[70] Z. I. Alferov, V. M. Andreev, E. L. Portnoi, and M. K. Trukan, "AlAs-GaAs heterojunction injection lasers with a low room-temperature threshold," *Sov Phys Semiconductors,* vol. 3, pp. 1107-1110, 1969.
[71] I. Hayashi, M. B. Panish, P. W. Foy, and S. Sumski, "Junction lasers which operate continuously at room temperature," *Applied Physics Letters,* vol. 17, pp. 109-111, 1970.
[72] H. Soda, K. Iga, C. Kitahara, and Y. Suematsu, "GaInAsP/InP surface emiting injection lasers," *Jpn. J. Appl. Phys.,* vol. 18, pp. 2329-2330, 1979.
[73] W. S. C. Chang, *Principles of Lasers and Optics*. UK: Cambridge University Press 2005.
[74] A. D. Broadbent, "A critical review of the development of the CIE1931 RGB color-matching functions," *Color Research and Application,* vol. 29, pp. 267-272, Aug 2004.
[75] R. W. Hunt, *Measuring colour*. England: Fountain Press, 1998.
[76] T. Smith and J. Guild, "The C.I.E. colorimetric standards and their use," *Transactions of the Optical Society,* vol. 33, pp. 73-134, 1931.

[77] J. P. Meyn, "Colour mixing based on daylight," *European Journal of Physics,* vol. 29, pp. 1017-1031, Sep 2008.
[78] J. Johansson, "Construction of a solid-state RGB laser," Master of Science, Department of Applied Physics, Royal Institute of Technology, Stockholm, 2007.
[79] S. F. Wen, "Design of relative primary luminances for four-primary displays," *Displays,* vol. 26, pp. 171-176, Oct 2005.
[80] G. Wyszecki and W. S. Stiles, *Color Science: Concepts and Methods, Quantitative Data and Formulas*, 2 ed. London: Wiley-Interscience 2000.
[81] T. Ajito, T. Obi, M. Yamaguchi, and N. Ohyama, "Expanded color gamut reproduced by six-primary projection display," *Projection Displays 2000: Sixth in a Series,* vol. 3954, pp. 130-137 242, 2000.
[82] M. Ou-Yang and S. W. Huang, "Determination of Gamut Boundary Description for multi-primary color displays," *Optics Express,* vol. 15, pp. 13388-13403, Oct 1 2007.
[83] T. Y. Fan, "Efficient Coupling of Multiple Diode-Laser Arrays to an Optical Fiber by Geometric Multiplexing," *Applied Optics,* vol. 30, pp. 630-632, Feb 20 1991.
[84] A. F. Kurtz, "Design of a laser printer using a laser array and beam homogenizer," San Diego, CA, USA, 2000, pp. 147-153.
[85] S. Holmstrom, A. D. Yalcinkaya, S. Isikman, C. Ataman, and H. Urey, "FR-4 as a new MOEMS platform," *2007 IEEE/Leos International Conference on Optical Mems and Nanophotonics,* pp. 25-26 203, 2007.
[86] S. O. Isikman, R. B. Sprague, and H. Urey, "FR4 Laser Scanner With Dynamic Focus," *IEEE Photonics Technology Letters,* vol. 21, pp. 233-235, Jan-Feb 2009.
[87] J. W. Goodman, "Some fundamental properties of speckle," *J. Opt. Soc. Am.,* vol. 66, pp. 1145-1150, 1976.
[88] G. Da Costa and J. Ferrari, "Anisotropic speckle patterns in the light scattered by rough cylindrical surfaces," *Appl. Opt.,* vol. 36, pp. 5231-5237, 1997.
[89] B. Gorbatenko, V. Ryabukho, and L. Maksimova, "Reconstructing an object image using the laser speckle pattern of the diffraction field," *Technical Physics Letters,* vol. 30, pp. 741-743, 2004.
[90] D. Q. Yu, M. Stern, and J. Katz, "Speckle noise in laser bar-code-scanner systems," *Applied Optics,* vol. 35, pp. 3687-3694, Jul 1 1996.
[91] L. L. Wang, T. Tschudi, T. Halldorsson, and P. R. Petursson, "Speckle reduction in laser projection systems by diffractive optical elements," *Applied Optics,* vol. 37, pp. 1770-1775, Apr 1 1998.
[92] P. Itay, Z. Michael, G. Boris, and K. Zvi, "MEMS Based Speckle Reduction Obtained by Angle Diversity for Fast Imaging," 2009, p. JTuD44.

[93] A. Furukawa, N. Ohse, Y. Sato, D. Imanishi, K. Wakabayashi, S. Ito, K. Tamamura, and S. Hirata, "Effective speckle reduction in laser projection displays - art. no. 69110T," *Emerging Liquid Crystal Technologies Iii,* vol. 6911, pp. T9110-T9110 120, 2008.

[94] F. Riechert, G. Bastian, and U. Lemmer, "Laser speckle reduction via colloidal-dispersion-filled projection screens," *Appl. Opt.,* vol. 48, pp. 3742-3749, 2009.

[95] M. N. Akram, V. Kartashov, K. Wang, G. Ouyang, and X. Chen, "Laser speckle reduction using a dynamic polymer-based diffraction grating spatial phase modulator," Beijing, China, 2009, pp. 73822H-9.

[96] S. C. Shin, S. S. Yoo, S. Y. Lee, C.-Y. Park, S.-Y. Park, J. W. Kwon, and S.-G. Lee, "Removal of Hot Spot Speckle on Rear Projection Screen Using the Rotating Screen System," *J. Display Technol.,* vol. 2, p. 79, 2006.

[97] F. Riechert, G. Craggs, Y. Meuret, B. Van Giel, H. Thienpont, U. Lemmer, and G. Verschaffelt, "Low-speckle laser projection with a broad-area vertical-cavity surface-emitting laser in the nonmodal emission regime," *Appl. Opt.,* vol. 48, pp. 792-798, 2009.